ISSN : 0019-5693

INDIAN JOURNAL
OF
THEORETICAL PHYSICS

VOLUME 70 **NOS. 1, 2**

JANUARY, 2022 – JUNE, 2022

Published by the
CALCUTTA INSTITUTE OF THEORETICAL PHYSICS
(Formerly, INSTITUTE OF THEORETICAL PHYSICS)
"BIGNAN KUTIR"
4/1, MOHAN BAGAN LANE, KOLKATA-700004

(Peer-reviewed Journal)

ISSN : 0019-5693

INDIAN JOURNAL
OF
THEORETICAL PHYSICS

[Founder President : Late Prof. K. C. Kar, D. Sc.]

VOLUME 70 **NOS. 1, 2**

JANUARY, 2022 – JUNE, 2022

INDIAN JOURNAL
OF
THEORETICAL PHYSICS

"BIGNAN KUTIR"
4/1, MOHAN BAGAN LANE, KOLKATA-70004, INDIA

SUBSCRIPTION RATE

INDIA : For Library (Institute)

₹1500.00 for each volume

FOREIGN : $ 350 for each volume

Drafts, Orders, Enquiries & Claim for Non-Receipt of Journal should be sent to :

CALCUTTA INSTITUTE OF THEORETICAL PHYSICS
(Formerly, INSTITUTE OF THEORETICAL PHYSICS)
"BIGNAN KUTIR"
4/1, MOHAN BAGAN LANE, KOLKATA-700004, India

C O N T E N T S

INDIAN JOURNAL OF THEORETICAL PHYSICS, VOL 70, NOS. 1 & 2, 2022

Density Functional Theory in Two-Dimensional Quantum Materials

M. Bora and P. Deb*

Department of Physics, Tezpur University (Central University)

Tezpur-784028, India

[Abstract: First principle-based density functional theory (DFT) has made tremendous impact on considering the properties and application of two-dimensional (2D) quantum systems. Available DFT simulation codes such as Quantum ESPRESSO (QE), Vienna *ab initio* simulation package (VASP) etc., can predict a wide range of energies, physicochemical, structural, vibrational, optical and spectroscopic, thermodynamic, magnetic phenomena. The structure-property correlation has evolved experimental findings by interpreting and analyzing the obtained experimental spectra. In this regard, validation of experimental findings of structure-property correlation via DFT simulation is an utmost important to realize the intrinsic nature of 2D quantum materials. Moreover, DFT is significantly increasing the demand because of its ability of discovering novel materials and their culmination of atomic structure addressing the long-lost limitation of identifying crystal polymorphs from its chemical composition. Here, we highlight the capabilities of DFT simulations with various properties required to understand the functionality of 2D quantum materials and the correlation with the experimental findings for its applicability in real-time scenario.]

*Corresponding Author : pdeb@tezu.ernet.in

1. Introduction

Designing and governing the quantum effects of atomically thin van der Waals (vdW) crystal endows basic realization of the underlying mechanism and interactions, which greatly influences in creating new functionalities such as Mott insulation, spin and valley-polarization, nontrivial phases, strongly correlated phenomena, structure-property correlation, thermoelectrics[1-8].The quantum confinement of electron in such atomically thin vdW crystal endues new physical paradigm that can be engineered by varying the parameters and sequence of the layered system[9]. These atomically thin vdW crystals have enormous potential in applied aspect such as environmental remediation, catalytic activity, energy storage, food packaging[10-15]. Despite a huge upsurge in material modelling, hunt for new vdW crystals and their systematic assessment of properties is still in improvement stage at the atomic and electronic level[16,17]. Therefore, there is an utmost need for high throughput approach using material modelling tool such as density functional theory (DFT), which has the competence of expecting the essential inherent properties of the quantum materials prior to the experimental realization and fundamental mechanism along with interactions involved in it [18].

The DFT is a fundamental premise including the motion and pair correlation to achieve electronic ground state, which primarily utters in terms of total electron density[19, 20]. Since the beginning, DFT gained enormous attention in realizing ground state electronic density, energy of any system such as clusters, solids, atoms and molecules in presence or absence of external perturbations[20]. The basis of DFT is based on Hohenberg-Kohn (HK) theorem[21], Kohn-Sham (KS) principle[22], local density approximation (LDA) and PAW method[23], generalized gradient approximation (GGA)[24] and pseudopotential (PP) method, which are

discussed in the present chapter for in-depth understanding of this *ab initio*-based simulation. These particulars required to contrive the basis sets in DFT simulation utilizing various packages such as QUANTUM Espresso[25]. DFT is a complementary approach to the traditional methods, which disentangle the complexities of many-body problem in quantum systems. Using DFT codes, graphene and other 2D materials such as transition metal dichalcogenides (TMDs) has been investigated for structural, vibrational, and electronic properties consuming LDA[26] and GGA with Perdew-Burke-Ernzerhof (PBE) functionals[24]. Moreover, DFT permeates the interlayer binding energies for atomically thin vdW crystals in the span of few meV/Å^2 [27]. Recently, DFT also simulates magnetic behaviour of vdW magnetic monolayers, hybrids and heterostructures[2-18, 10-15, 39, 53]. In this regard, using the contemporary computational codes becomes challenging task to achieve the electronic properties considering a many-body problem for quantum materials (functional as well as structural).

As evident from aforementioned discussion, a complete quantum-mechanical approach of a system is required considering nuclei and electronic wave functions; however, the mass of an atomic nucleus is much higher than that of mass of electron. The *ab initio* based technique has huge impact in modelling and determining properties of atomically thin vdW crystals with its application aspect. In this review paper, we try to highlight the promising aspects of First-principle based DFT in determining energetic stability, electronic, magnetic, topological properties along with their potential applications in atomically thin vdW crystals and there heterostructure s. The aforementioned properties can be described within the framework of DFT, which is validated at $T = 0\ K$ and intrinsic behaviour of quantum materials can be speculated and remains consistent over the extent of electronic wave functions. Additionally, we correlated DFT simulated

results with experimental findings for in-depth and comprehensive understanding in structure-property correlations of quantum systems. Finally, we describe the advantages and properties that can be investigated using DFT as a tool for atomically thin vdW heterostructure in various applications.

2. Density functional theory methods

Initially, the strongly correlated electron system was explained by Thomas-Fermi (TF) model[28, 29] and Hartree-Fock-Slater[30] method, which are the ancestor of latest DFT method. As per the TF model, the class of system containing interacting electrons without relativistic effect in Schrödinger equation can be written as,

$$H \equiv \hat{T} + \hat{U}_{en} + \hat{U}_{ee} \quad \ldots (2.1)$$

$$H = -\frac{1}{2}\sum_j \nabla_j^2 + \sum_j u_{ext}(\boldsymbol{r_j}) + \frac{1}{2}\sum_{j\neq k}\frac{1}{|\boldsymbol{r}_j - \boldsymbol{r}_k|} \quad \ldots (2.2)$$

Here, $\hat{T} = -\frac{1}{2}\sum_j \nabla_j^2$ denotes the kinetic energy operator, $\hat{U}_{en} = \sum_j u_{ext}(\boldsymbol{r}_j)$ is potential energy due to electron-nuclei interaction and $\hat{U}_{ee} = \frac{1}{2}\sum_{j\neq k}\frac{1}{|\boldsymbol{r}_j - \boldsymbol{r}_k|}$ is potential energy due to electron-electron interaction. With the help of TF approximation, the kinetic energy *T[n(r)]* is approximated for a non-interaction system with electron density *n(r)*. In TF model, the exchange-correlation energy term is ignored and the Hartree approximation remains identical to TF model. In this regard, this technique fails to realize the shell model and stabilization of molecules.

The aforementioned shortcomings can be overcome by generalizing the TF model implementing in modern DFT approach. The modern DFT approach is found to be an exact approach for solving many-electron problem. This approach solves the set of equations via iterative scheme, which is based preferably on KS scheme. The precursor to modern DFT

approach is associated with the previous work of Thomas[29], Fermi[28], Dirac[31], von Weizsacker[32] and Slater[33]. The beginning of DFT approach was evolved from the ground-breaking research of Hohenberg and Kohn in the year 1964[21] and Kohn and Sham in 1965[22]. The HK theorem published in 1964 describes that the energy ground state is a functional of electron density, where combination of energy and electron density can be acquired by minimizing the energy as a function of the density at fixed functional. The paper published in 1965 set a stage to form the electronic ground state density by considering non-interacting orbitals, basically the KS wave functions. The preliminary understanding of the HK theorem and KS scheme constructs the ideal system for non-interacting Fermions having density *n(r)* equivalent to interacting Fermions. Taking into account the superiority of both the works, the respective theorems are explained below for detail understanding.

2.1 Hohenberg-Kohn Theorems

The first theorem states as: *The ground state energy E_0 is the unique functional of the ground state electron density* $E_0=<\Psi_0[n_0]|H|\Psi_0[n_0]>=E_0[n]$.

The Coulombic potential present between electrons for determining the electronic nature of solids, basically depends on HK functional. Moreover, the interacting nucleus, molecules, crystals depend on the effective potential operator. Therefore, the HK functional is named as unique functional, because it attains constant value for all systems. The non-degenerate ground state electron density can be constructed from the Hamiltonian operator, which determines the information of expectation values for all states of the system.

The second theorem states as: *The ground state energy E_0 can be proved via Variational principle: the electron density n(r), that minimizes the total energy, is the true ground state energy $E_0[n_0] \leq E[n]$.*

The external potential universally constructs the ground state wave functions, which establishes all observables of the system such as kinetic energy. Moreover, the HK theorems are expanded to more crystal systems and dimensions from bulk to low-dimensions, which incorporates various parameters such as SOC, spin-polarization etc. Moreover, HK theorems are extremely robust, but practically they do not have any provision to compute the ground state electron density. In this regard, Kohn and Sham provides a simple iterative method scheme for performing *ab initio* DFT calculations.

2.2 Kohn-Sham approach

Kohn and Sham advocate the following scheme:

The theorem formulates that for each interacting system S with distinct functional, there exist non-interacting system R, described by Hamiltonian $\widehat{H_S} = \hat{T} + \hat{V}_S$, where $\hat{V}_S$ yields the same true ground state electron density $n_S(r)=n_R(r)$.

The HK theorem determines uniquely the ground state electron density of the system. It is important to obtain suitable potential energy to describe the electron density $n_R(r)$. The additional system exhibits non-interacting kinetic energy functional; the density of that energy functional collects from single-particle equation to obtain KS orbitals. The single-particle equation relies on the electron density *n(r)*, also depends solely on KS orbitals. In this regard, it is important that the single-particle equation must be solved self-consistently by means of iterative scheme. The ground state energy and electron density can be obtained exactly, if the exchange-correlation (X_C) term is exactly recognized. It is necessary to know the

exact value of X_C term, because it has all the quantum mechanical origin for various fictitious non-interacting and interacting systems. Therefore, it has an utmost need to find an appropriate and descent approximation to determine the X_C term.

2.3 Exchange-Correlation term

The KS-DFT approach is mainly to solve many-electron Schrödinger equation by separating out the discrete single-particle kinetic energy term and Hartree term from the interacting X_C functional. However, an appropriate discussion on X_C functional can be understood by quantum mechanical adiabatic process. The Hamiltonian for electron density varies adiabatically to reach the ground state more rapidly than the motion of nucleus. The X_C term accounts for remaining interacting and non-interacting kinetic and electrostatic terms, which creates a bridge by determining the scaling factor (ξ) to obtain the electron-electron coupling term. The interacting and non-interacting terms are transformed between 0 and 1, where density is constant under adiabatic process. This inference suggests the equation for exchange-correlation energy term,

$$E_{XC}[n(r)] = \frac{1}{2}\int n(r)dr \int \frac{n_{XC}(r,r')}{r-r'}dr' \qquad \ldots (2.3)$$

Here, $n_{XC}(r, r')$ corresponds to the average X_C interaction factor. Thus, we can determine the exchange-correlation density as,

$$\in_{XC}[n(r)] = \frac{1}{2}\int \frac{n_{XC}(r,r')}{|r-r'|}dr' \qquad \ldots (2.4)$$

The n_{XC} term can be decomposed into two disparate parts expressed as $n_{XC}(r,r') = n_X(r,r') + n_C(r, r')$, where $n_X(r, r')$ is the exchange term and $n_C(r, r')$ is correlation term obtained linearly. The exchange term (n_X) can be characterized by considering the Hartree-Fock (HF) energy term as,

$$E_{XC}[n(r)] = \frac{1}{2}\int n(r)dr \int \frac{n_X(r,r')}{r-r'}dr' \quad \ldots(2.5)$$

The exchange-correlation term X_C can be described as $E_{XC} = \int n(r) \in_{XC} [n(r)]dr$. The true ground state can be obtained by employing the approximations to know the exact X_C functional. It is important to realize exchange-correlation density for each electron to construct appropriate approximations to realize the quantum mechanical origin.

2.4 The Plane-wave Pseudopotential approach

To introduce DFT practically on real systems, it is essential to solve KS equations in a computationally efficient way *via* iterative scheme with highest accuracy in the results. The calculation carried out in all the chapters of this thesis considers the plane wave pseudopotential method to solve the KS equations. This method involves plane wave basis set to characterize the atomic orbitals and pseudopotential designate the nucleus and core electrons. Alternative methods to describe plane wave pseudopotential does exist in simulations include localized basis function for sole atomic orbitals[34]. Although the alternate methods are computationally favourable, but these methods suffer due to incomplete basis set creating hindrance in obtaining truly converged ground state energy as a function of basis set. In this regard, plane wave pseudopotential approach is highly considerable over the alternate basis sets. Combination of plane waves with pseudopotential can extensively modify the exactness of DFT calculation. Currently pseudopotential, also known as effective potential, constructed from first-principles calculations by solving KS equation and simplifies the information regarding complex systems. The manifestation of pseudopotential gives an effort to modify the complication of the motion of core electrons and nucleus creating an effective potential term, which modifies the Schrödinger equation instead of Coulomb potential term. The

atomic orbitals exhibiting spherical symmetry conduct the task and express its wave function as the product of radial and spherical function. The Schrödinger equation can be solved by reducing to one-electron particle considering radial function by integrating numerically. A schematic illustration of corresponding many-electron wave function expressed with respect to Coulomb potential shown in Figure 2.1. The prime motive is to reduce many-electron problem within a sphere of effective potential having core electrons with radius $r_{cut\text{-}off}$ by a debilitated potential having same ground state wave function for similar energy eigen value as the initial many-electron wave function outward $r_{cut\text{-}off}$ (shown in Figure 2.1 with dotted line). Pseudopotential with higher electron core cut-off radius is softer, which converges more promptly.

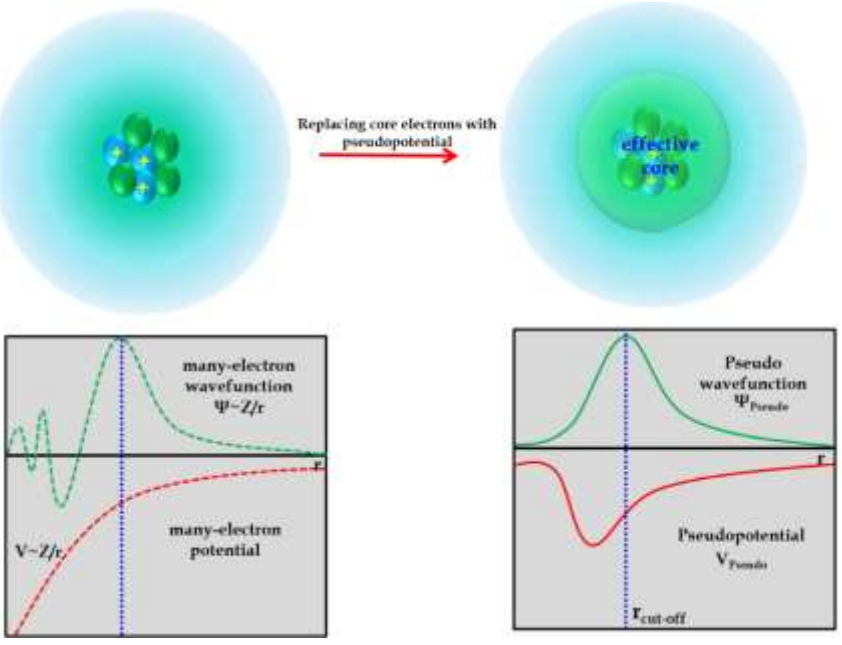

Fig. 2.1: Displaying the schematic representation of many-electron wave function shown in green dashed line and corresponding pseudo wave function, Ψ_{Pseudo} (green solid line) combining with Coulomb potential shown in red dashed line and pseudopotential (red solid line).

The concept of pseudopotential approximation was first introduced in 1934 by Hans Hellmann. The commonly used pseudopotential in modern DFT is norm conserving pseudopotentials (NCPP) and ultrasoft pseudopotential (USPP). The former pseudopotential basically includes the creation of nodeless pseudo wave function Ψ_{Pseudo} by conserving the norms of many-electron wave functions. These pseudopotentials commonly allow basis-set by considering lower cut-off energy for describing the electronic wave functions with proper convergence with reasonable computing resources. However, NCPP was first introduced in 1979 by Hamann, Schl*ü*ter and Chiang (HSC)[35]. The norm conserving pseudopotential generates by inverting the Schr*ö*dinger equation at many-electron Eigen values, given as

$$\left[-\frac{\hbar^2}{2m_e}\nabla^2 + V_l(r) - \in \sim \frac{Z}{r}\right]\Psi \sim \frac{Z}{r}(r) = 0 \qquad \ldots (2.6)$$

$$\hat{V}_l(r) = \sum_m \sum_n |Y_{mn} > V_{mn}(r) < Y_{mn}| \qquad \ldots (2.7)$$

The norm-conserving pseudopotential acquired here is semi-local with high degree of tunability, which performs utilizing single-electron wave functions in the similar manner. However, to minimize computational cost Kleinman and Bylander[36] reframed the equations independently in non-local form. The challenge remains when all elements are treated with nodeless valence electrons within pseudopotential framework. In this case, the wave functions of pseudopotential and many-electron must be commensurate. The electrons in valence state are predominantly localized in ionic core making it computationally expensive for carrying out the calculations. To overcome the limitation of NCPP, Vanderbilt developed an advanced pseudopotential named Vanderbilt ultra soft pseudopotential (USPP), where the need of

including ionic cores has been relaxed[37, 38]. In this case, USPP considers small portion of wave function, which is simulated instead of illustrating the full potential wave function using plane waves. This helps in reducing the cut-off energy of plane wave in the simulations. The compensation in plane wave cut-off energy lowers the cost of computation in many other computational efforts needed for improvement.

2.5 Properties of 2D quantum materials

Advances in scaling down with 2D quantum materials lead to improved functionality that is ambiguous from bulk counterparts. This ambiguity is mostly evident from the transformation of electronic structure when it comes to monolayer. In addition, 2D material comprises of surfaces and interfaces which later can be altered by forming heterostructure by proximity effect[2, 4, 5], adding heteroatoms over the surface[11, 12] and dopants[39] can vividly vary the intrinsic properties of the pristine system. The exclusivity 2D quantum materials reveal possibly useful properties such as high carrier mobility[6], topologically active states[2, 3], tunable electronic structure[5], high electronic thermal conductivities[7] and its application in spintronics and valleytronics[2,3,5], quantum energy storage[12], catalysis[40]. In this regard, First-principle DFT simulation provides an effective tool to approach and solve the above-mentioned alteration in structure-property correlation in atomically thin vdW materials. This section will offer a comprehensive overview of DFT simulation of the various properties of 2D quantum materials.

2.5.1 Electronic properties

One of the utmost importance in DFT is to achieve ground state energy at T = 0 K with the coordinates characterize by atomic positions and atomic numbers for amplified quantum system by maintaining its

periodicity of crystal system. DFT quantifies the atomic coordinates which is reliable for approaching electronic properties calculation. First, DFT merely depends on single-particle wave functions creating the periodicity to be direct and simpler. Second, DFT employ plane-waves along with pseudopotentials having effective scaling for distinctive sizes of system comprising N number of atoms[41]. The electronic properties and modelling of 2D quantum materials are characterized by density of states (DOS), electronic band structure, and charge density distribution as shown in figure 2.2. The optimized interlayer spacing and atomic structure is obtained by simulating the ground state energy using Feynman-Hellman theorem under the framework of density functional theory as shown in figure 2.2 (a) and (b). The interlayer spacing between graphene and ferromagnetic $CrBr_3$ is 0.13 Å displaying in figure 2.2 (b). Figure 2.2 (a) is modelled in such a way where A and B are contrasting sublattices, where optimized ground state energy is obtained for vdW heterostructure system. The optimized ground state energy is achieved when ferromagnetic ordering is considered using PBE-GGA exchange and correlation functional[42]. Figure 2.2 (c) shows the spin-polarized partial density of states (PDOS) for Gr-$CrBr_3$ vdW heterostructure . It is evident from the figure 2.2 (c), the total spin-polarization is found to be 63.6% in the heterostructure system which is higher than the pristine systems. Figure 2.2 (e) shows the semimetal-semiconductor characteristic of the vdW heterostructure system, which also signifies the modelling of the atomic structure using PBE-GGA functional and exchange term U (Coulomb interaction) for 3d electrons of chromium atom precisely accurate and cancels the self-interaction between an electron and own charge density. The blue and cyan continuous lines signify spin-up and down bands, respectively[2, 5]. Figure (h) and (i) shows the HRTEM micrographs of graphitic carbon nitride (g-C_3N_4) and g-C_3N_4@$FeNi_3$with an

inset of the atomic configuration of heterostructure system. These systems show promising electrochemical behaviour having its suitability in developing planar micro-super capacitor for quantum energy storage capacity. As expected, we notice the changes in LDOS (figure 2.2 (j)) where monolayer g-C_3N_4 have a band gap and transforms to metallic in case of multilayer. Moreover, the heterostructure system shows metallic behaviour in monolayer as well as multi layeras shown in figure 2.2 (k) using the same exchange-correlation functional represented by projector augmented wave (PAW) pseudopotentials[23]. Figure 2.2 (f) and (g) corresponds to multilayer g-C_3N_4 and g-C_3N_4@$FeNi_3$, which corroborates well with figure 2.2 (j) and (k) [12]. Figure 2.2 (l) and (m) corresponds to the electronic band structure of monolayer black phosphorus (MLBP) simulated at 300 and 500 K. The inset shown in figure 2.2 (m) describes the atomic configuration of MLBP with an optimized structure by means of quasi Newtonian algorithm using *ab initio* DFT simulation. It is noticed that the trend of band gap is consistent with metallic nature at room and high temperature using PBE-GGA functional with PAW pseudopotential which later-on combining with density functional perturbation (DFPT) theory analyses the phonon dynamics of 2D quantum system[6]. It is also important to mention that there is hybrid functionals such as HSE06, SCAN, optB88 used for simulating various properties such as electronic, optical etc for more accuracy. However, the hybrid functionals are computationally heavy and expensive; in such case PBE-GGA functional is computationally efficient and varies the density regimes for hybrid interfaces[24, 43].

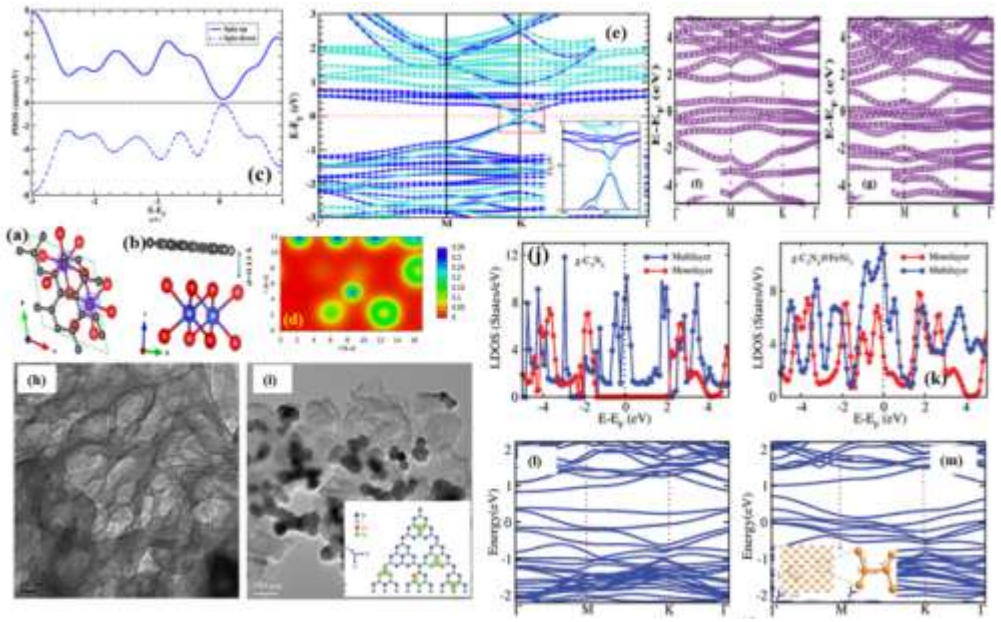

Fig. 2.2:Atomic configuration of Gr-$CrBr_3$ vdW heterostructure (a) Top-view of Gr-$CrBr_3$ heterostructure in unit cell. (b) Side view of the heterostructure with an interlayer spacing of 0.13 Å. The grey, blue and red spheres correspond to carbon (C), chromium (Cr) and bromine (Br) atoms, respectively. (c) Spin-polarized total partial density of states (PDOS) of the heterostructure system. (d) Charge density distribution of Gr-$CrBr_3$ bilayer system. (e) Spin-polarized dependent electronic band structure of heterostructure system. The blue and cyan continuous line displays spin-up and down configuration, respectively. Inset displays the topologically preserved Dirac cone at the Fermi level. Electronic band structure of multilayer (f) g-C_3N_4 (g) g-C_3N_4@$FeNi_3$ heterostructure composite along high-symmetry point Γ-M-K-Γ.HR-TEM micrograph of (h) g-C_3N_4 (i) g-C_3N_4@$FeNi_3$ heterostructure composite. Local density of states (LDOS) for monolayer and multilayer (j) g-C_3N_4 (k) g-C_3N_4@$FeNi_3$ heterostructure composite system. The band structure at (l) 300 K (m) 500 K of monolayer black phosphorus (MLBP).

2.5.2 Magnetic properties

Understanding magnetic behaviour solely has no particular theoretical method instead it is a quantum mechanical phenomenon, where DFT is one

of the most effective theoretical tools to govern the magnetic phenomena in solid state. Under the framework of DFT, magnetic properties can be characterized by quantities such as magnetic moment, magnetic ordering, and direction of magnetization, non-collinear case and spin-orbit coupling (SOC) at ground state. In non-SOC case, the magnetic moment is stated by considering scalar quantities where the overall energy of the system remains unchanged to the spin rotation of crystallographic variable cell. In SOC case, the computation cost is 1-2 magnitude higher because of considering complete spin-density matrix and symmetry breaking of quantum materials[44]. This limitation can be overcome by incorporating self-interaction correction (Hubbard Parameter, U) in the input of the DFT calculation. Few studies in achieving the ground state energy with magnetic ordering has been established to articulate the spin related phenomena in 2D quantum materials. Figure 2.3 (a) shows electronic band topology of Gr-$CrBr_3$ heterostructure system in presence of SOC, where a global band gap is opened at the Fermi level as compared to non-SOC case shown in figure 2.2 (e). The magnetic moment obtained for the heterostructure system and monolayer $CrBr_3$ is 3.47 μ_B per cell and 3.39 μ_B per cell, respectively. It is seen that the magnetic moment is increased up to 8% in the heterostructure and 39% in the monolayer relative to the bulk counterpart. The DFT+U parameter is incorporated along with non-collinear input in the simulation of Gr-$CrBr_3$ vdW heterostructure . Figure 2.3 (b) displays the projected density of states of the heterostructure system with the inclusion of SOC. It is evident that orbital contribution of individual atoms of the heterostructure system. The spike nature of PDOS pattern ventures the presence of ferromagnetic ordering due to magnetic proximity effect in hetero-bilayer system[2, 5]. Figure 2.3 (c) describes the crystal structure of 1T-VSe_2/1H-$MoSe_2$ vdW heterostructure system. The ground state energy is achieved

when ferromagnetic ordering is considered in the system. Figure 2.3 (d) shows the PDOS for the individual atoms orbital contribution, where the magnetic ordering is basically due to the presence of $3d^3$-$4s^2$ orbitals of vanadium (V) atom. Figure 2.3 (e) displays the density of states for 1T-VSe_2/1H-$MoSe_2$ heterostructure where spike like nature is clearly evident speculates the presence of magnetic ordering. It is also seen that the spin-up states relative to spin-down states are not matching, constructing an asymmetric behaviour with metallic nature near the Fermi level. Moreover, the asymmetric nature reveals the magnetic behaviour of the heterostructure system with net spin preservation that confirms the presence of magnetic moment. The collinear self-consistency achieves total magnetic moment of 2.64 μ_B per cell in the heterostructure system[3]. It is seen from the studies that DFT appears to be a good candidate for initial theoretical determination of the magnetic landscape in low-dimensional quantum systems.

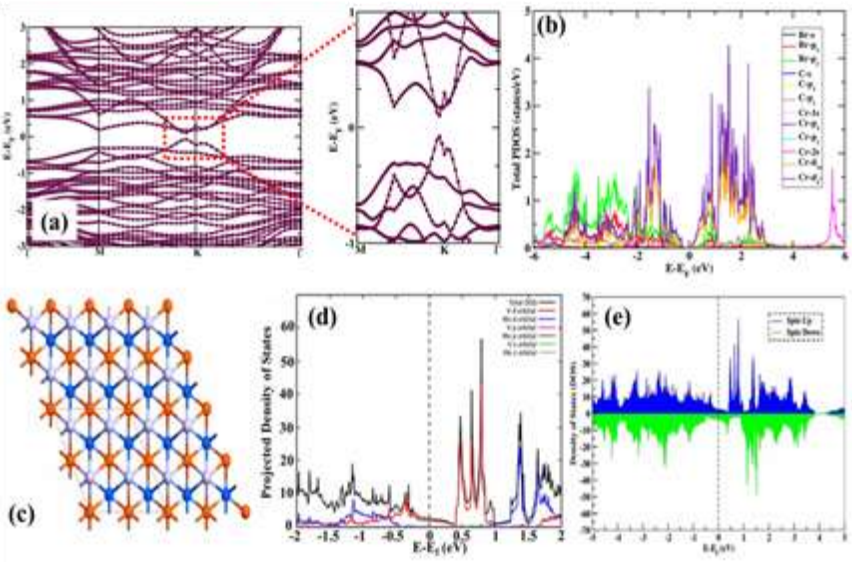

Fig 2.3: (a) Electronic band structure of Gr-$CrBr_3$ vdW heterostructure with the inclusion of spin-orbit coupling (SOC). The magnified image shows band topology at Fermi level. (b) Spin-polarized PDOS of Gr-$CrBr_3$ vdW heterostructure in

presence of SOC. Crystal structure of 1T-VSe_2/1H-$MoSe_2$ vdW heterostructure (c) Top-view of AB stacked super cell. The orange, blue and white spheres are vanadium (V), molybdenum (Mo) and selenium (Se), respectively. (d) Collinear PDOS with atomic orbital contribution and (e) total density of states without implementation of SOC.

2.5.3 Topological properties

Topologically non-trivial phases in 2D quantum materials have been fascinating due to their potential application in spintronics and valleytronics[45]. To realize the topological phenomenon in such quantum systems, the incorporation of relativistic effectsact as an important element in characterizing electronic, magnetic, and topological properties. These effects are classified into scalar-relativistic (SR) associated to mass-velocity and Darwin terms, and the fully-relativistic considering SOC. The second term provides various physical phenomena such as Dresselhaus[46], Rashba effects[47], and spin Hall Effect[48]. The fundamental mechanism for occurrence of topologically active states in 2D quantum materials is because of spin-orbit interaction (SOI)[49]. Therefore, it is necessary to treat the problem of SOI by considering *ab initio* methodologies. Recent DFT-based studies with maximally localized Wannier function (MLWF) approach[50] have been investigated with the implications of SOC, which validates the occurrence of quantum phenomena in vdW heterostructure system. Figure 2.4 (a)shows the collinear electronic band structure of 1T-VSe_2/1H-$MoSe_2$ vdW heterostructure , whereas figure 2.4 (b) displays the corresponding magnified image of figure 2.4 (a) with crossing of bands. With inclusion of SOC, a small gap of 10 meV is observed in figure 2.4 (c) and (d) corresponding to non-trivial band topology. The calculation of Z2 invariant number is obtained for six momentum planes (shown in figure 2.4 (e) [i-vi])by interfacing DFT and MLWF. In figure 2.4 (e) [i-iv] shows no

crossover of the reference line (green dashed line) whereas the reference line (green dashed line) is crossed once along the k_z plane as shown in figure 2.4 (e) [v-vi]. This also confirms from figure 2.4 (f) where evolution line of Wilson loop crosses the reference line (green dashed line) once depicting the Chern number value of the heterostructure system to be 1^3. In another case, the evolution of Wilson loop and Berry curvature is observed for Gr-$CrBr_3$ vdW heterostructure . It is seen in figure 2.3 (a), the opening of global band gap at Fermi level further characterizes the Berry curvature to be non-zero. Figure 2.4 (g) shows the Berry curvature to be inverted and peaked at valley K and K', respectively. The presence of positive and negative value in Berry curvature leading to valley Chern number to be 1. This is also evident from figure 2.4 (i) with the implications of SOC the evolution line has crossed once the reference line (red continuous line) as compared to non-SOC case where no crossing of evolution line is seen as shown in figure 2.4 (j). The inverted and peaked valley at K and K' can be corroborated with Berry density plot shown in figure 2.4 (h) which acts like a source and sink of Berry curvature. This clearly signifies the presence of topologically non-trivial phase and valley contrasting anomalous behaviour. Figure 2.4 (k) displays the anomalous Hall conductivity of Gr-$CrBr_3$ vdW heterostructure system. The red dot-dashed lines mark the extreme maxima of valley K and K' suggests the existence of valley contrasting anomalous Hall effect[2]. Apart from inclusion of SOC, 2D quantum materials has high degree of tunability with application of external perturbative effect such as electric field, strain, and pressure[51, 52]. Figure 2.4 (l) and (m) shows the phase diagram of obtaining Z2 topological invariant with the inclusion of electric field in electronic band structure of hexagonal boron nitride (h-BN)/Gr/h-BNsymmetric and asymmetric trilayer vdW heterostructure system, respectively[53].

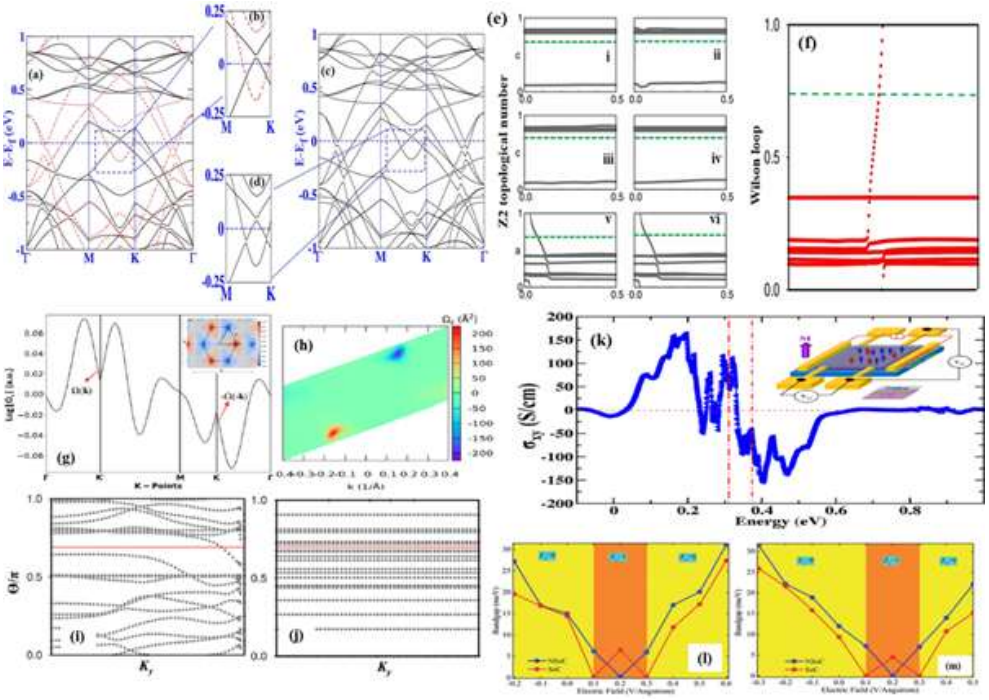

Fig. 2.4: Energy band topology of 1T-VSe_2/1H-$MoSe_2$ vdW heterostructure (a) non-SOC. The red dashed and black solid lines correspond to spin-up and down states, respectively. (c) with implications of SOC. The magnified image displays (b) the band crossover, (d) band gap of 10 meV. (e) Represents the Z_2 invariance along (i) k1 = 0.0, Z_2 = 0; (ii) k1 = 0.5, Z_2 = 0; (iii) k2 = 0.0, Z_2 = 0; (iv) k2 = 0.5, Z_2 = 0;(v) k3 = 0.0, Z_2 = 1; (vi) k3 = 0.5, Z_2 = 1 momentum planes. (f) Wilson loop for 1T-VSe_2/1H-$MoSe_2$ vdW heterostructure with the inclusion of non-collinear relativistic effect. (g) The Berry curvature plot of Gr-$CrBr_3$ vdW heterostructure system along the high-symmetry points. The red dashed arrows show Ω(k) and -Ω(-k) (in logarithmic scale). Inset shows the first Brillouin zone of Berry curvature in 2D k-plane. (h) Berry density plots for the first Brillouin zone of heterostructure system. (i) Evolution of Wilson loop for Gr-$CrBr_3$ hetero-bilayer system with inclusion of SOC (j) without SOC. The red solid line shows the reference line. (k) The calculated anomalous Hall conductivity with respect to energy. The red dot-dashed lines show the two valleys. Inset shows the device architecture of quantum valley Hall (QVH) effect in the vdW heterostructure system.

2.5.4 Catalytic properties

Catalytic activity is the quantum chemical method where the chemical reaction takes place between surface and interface explaining the adsorption mechanism and surface conversion of 2D vdW systems[54, 55]. In this line, theoretical approach has become rigorous due to the clarification of spectroscopic data and validation of catalytic mechanism, which models the chemical reaction pathways and chemical reactivity.In this regard, DFT-based calculations improve the understanding on homogeneous chemical reactions, heterogeneous catalysis, surface science, and electrochemical activity[56]. The adsorption process in Al_5Mg_2 cluster has been simulated under DFT framework using PBE-GGA functional as the basis method[57]. The energy barrier and reaction pathways of the system can be described by nudget-elastic-band (NEB) approach[58]. The complexity increases in electronic structure of such cluster based systems, which creates steric hindrance and later on act like a macromolecules. In this regard, the lattice of 2D quantum materials and the interface between the 2D surface and the active constituent deliver important confining milieu for active sites, which encourage new perspective of confinement catalysis with 2D quantum materials[59]. Experimentally established g-C_3N_4/CuSe hetero interface for photo catalytic activity have been carried out for which ab initio based DFT study is incorporated to validate the catalytic activity of the heterostructure system. Figure 2.5 (a) and (b) displays the crystal geometry of g-C_3N_4/CuSe and g-C_3N_4/CuSe-Methylene blue (MB) heterostructure system, respectively. The ground state energy of the heterostructure system is achieved by considering vdW correction proposed by Grimme[62]. The total surface energy value for g-C_3N_4/CuSe-MB is -1582.57 Ry whereas for pristine system without MB the total surface energy value is -1205.22 Ry. This confirms heterostructure system in presence of MB molecule have

higher stability than the pristine system without MB molecule. Figure 2.5 (c) and (d) displays the DOS pattern of g-C_3N_4/CuSe and g-C_3N_4/CuSe-MBto realize and control the dynamic nature of the active sites present in the heterostructure system. The overlapping and metallic nature is clearly evident from the DOS pattern of the systems. The presence of copper (Cu) and selenium (Se) atoms trigger the metallicity at the Fermi level in the heterostructure systems. As a consequence, the electrons localized above the surface of g-C_3N_4 and obtained metallicity along with the conduction band (CB) and enhanced kinetic energy suggests the delocalized activity of the active sites. Figure 2.5 (e) displays the planar-averaged electrostatic potential along z-directions for the heterostructure systems. The potential drop of 4.04 eV is clearly evident through the CuSe and g-C_3N_4 interface, controlling the charge transfer from CuSe to g-C_3N_4 system. The potential drop clearly shows the robustness of electrostatic field strength at the interface, which speculates the effect of carrier mobility and charge transfer in the heterojunction and fasten the dye degradation mechanism also seen in figure 2.5 (h-j). Figure 2.5 (f) shows the layered morphology of g-C_3N_4/CuSe heterostructure system. The wrinkled layers of g-C_3N_4 are observed along with the agglomerated plates of CuSe. The junction produced between g-C_3N_4 and CuSe will accelerate the separation of photo excited carriers in photocatalytic mechanism. Figure 2.5 (g) depicts the UV-visible light spectrum of the heterostructure system. The UV absorption band edge of heterostructure system is found to be 402 nm. The inclusion of CuSe plates into g-C_3N_4 suggests the Frenkel exciton dissociation, which widens the range of visible light spectrum. The inset determines the corresponding band gap of g-C_3N_4@CuSe estimated to be 0.77 eV. This confirms the band gap of the heterostructure squeezes tending to metallicity when combined with g-C_3N_4 due to which the photocatalytic activity is

boosted. Figure 2.5 (h-j) displays the complete decolouration of MB dye occurs within 15 minutes for the g-C_3N_4/CuSe heterostructure system. In order to validate the photo catalytic activity of the heterostructure system, the *ab initio* DFT simulation is taken into consideration. Figure 2.5 (l-q) reveals the band alignment diagrams using three different functionals PBE (figure 2.5 (l,o)), meta-GGAC (figure 2.5 (m, p)), and Heyd-Scuseria-Ernzerhof (HSE) (figure 2.5 (n, q)) hybrid functional for the heterostructure system without MB (top panel of figure 2.5 (l-n)) and with inclusion of MB (lower panel figure 2.5 (o-q)), respectively. The calculation of these band alignments in nanoscale regime requires numerous steps to realize the involvement of individual atoms on the proximitized interface and planar averaged electrostatic potential of the pristine solids in any heterojunction[40]. Figure 2.5 (r-t) shows stable atomic configuration of isolated molybdenum sulphide (MoS_2) layer, isolated graphene layer and isolated nitrogen doped graphene layer, respectively. Figure 2.5 (u, v) shows the pristine hetero-bilayer system and nitrogen-doped hetero-bilayer, respectively. Figure 2.5 (w, x) displays the trilayer of Gr/MoS_2/Gr and N-Grp/MoS_2/N-Grp, respectively. Figure 2.5 (y) depicts the free energy diagram[60] at over potential U=0 eV to describe the steps to achieve hydrogen evolution reaction (HER) process using NEB approach under DFT framework. The trilayer system N-Grp/MoS_2/N-Grp shows high value of free energy due to increased conductivity and higher surface area of the heterostructure system. Figure 2.5 (z) depicts the electro catalytic and HER activity in terms of hydrogen coverage for bilayer and trilayer heterostructure systems. It is evident that nitrogen doped layers are forecasting enhanced HER performance as calculated from Gibb's free energy[61].

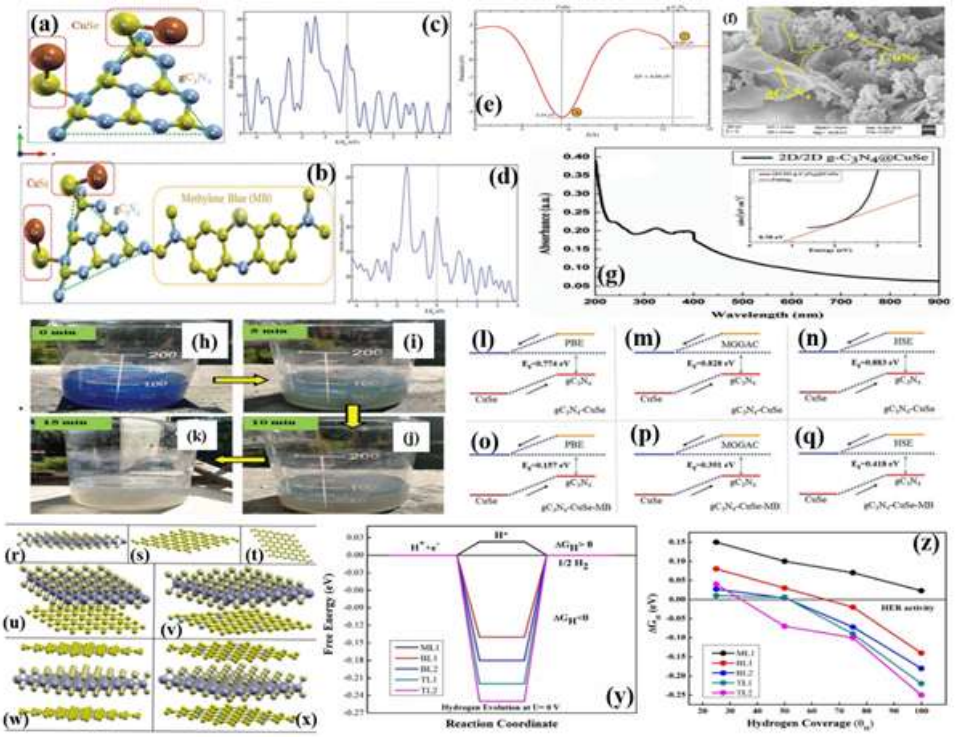

Fig. 2.5: Crystal geometry of (a) pristine g-C_3N_4/CuSe heterostructure and (b) g-C_3N_4/CuSe-MB with naming each single atom. Red-dotted box shows the presence of CuSe in the variable cell simulation, green dotted triangle portion shows g-C_3N_4, while yellow marked box shows the presence of MB.Density of states (DOS) pattern for (c) g-C_3N_4/CuSe and (d) g-C_3N_4/CuSe-MB. (e) Planar averaged electrostatic potential for g-C_3N_4/CuSe vdW heterostructure system. Positive value depicts electron accumulation (negative charge and n-type conductivity) and negative value shows electron depletion (positive charge and p-type conductivity). (f) FESEM image of g-C_3N_4/CuSe. Yellow dashed area reveals the interface between g-C_3N_4 and CuSe. (g) UV-Visible spectrum of g-C_3N_4/CuSe heterojunction. (h-j) Real time pictures of MB dye degradation under the exposure of sunlight. Band alignment diagram of the heterojunction (top panel (l) to (n)) for g-C_3N_4/CuSe and (lower panel (o) to (q)) for g-C_3N_4/CuSe-MB. Crystal structure of (r) monolayer (ML) MoS_2, (s) ML graphene, (t) ML nitrogen-doped graphene, (u) bilayer (BL) MoS_2-graphene heterostructure , (v) BL MoS_2-nitrogen doped

graphene, (w) trilayer (TL) graphene-MoS_2-graphene, (x) TL nitrogen doped graphene-MoS_2-nitrogen doped graphene. (y) Free energy diagram of HER reaction of the heterostructure system. (z) DFT calculated Gibb's free energy with respect to hydrogen coverage for pristine and corresponding nitrogen doped heterostructure active sites.

Conclusions and Outlook

In this review, we have highlighted *ab initio*-based density functional theory (DFT) approach as a prevailing tool for understanding and predicting wide range of properties from energies and modelling atomic configurations to reaction pathways and van der Waals interactions in two-dimensional (2D) quantum materials and their heterostructure s. Advances in scaling quantum materials by solving quantum mechanical equations as a function of size restricts their novel aspects in understanding coupled systems like 2D vdW heterostructure s. In this regard, solving many-body problem quantum mechanically from DFT and maximally localized Wannier function (MLWF) approach, are one of the substantial tools to investigate electronic, topological and magnetic properties of vdW quantum systems. For solving HK and KS theorems, DFT is legitimately precise technique for calculation of electronic properties using pseudopotential plane wave basis sets. While MLWF method rely on localized Wannier basis sets with coarse real-space grid using full potential basis sets. Thus, integration of DFT and MLWF provides an exact accuracy and reducible simulation to achieve various properties of complicated vdW quantum systems, where the computational cost becomes less expensive. This creates a bridge between First-principles simulations and MLWF for determining various properties (topological, magnetic, electronic and catalytic) of strongly correlated systems.

Acknowledgement

M.B. and P.D. acknowledge Indian Institute of Technology, Kharagpur and Tezpur University for HPC cluster computing facility. P.D. thank NBIOs award project, Department of Biotechnology, Govt. of India, vide grant no. 102/IFD/SAN/3183/2021-22.MB (IF180514) acknowledges Department of Science & Technology (DST), Govt. of India for providing financial support as INSPIRE fellowship.

References

1. Zunger, A. - Bridging the gap between density functional theory and quantum materials, Nat. Comp. Sci. **2**, 529-532 (2022).
2. Bora, M., Behera, S. K., Samal, P., Deb, P. – Magnetic proximity induced valley-contrasting quantum anomalous Hall effect in a graphene-CrBr3 van der Waals heterostructure , Phys. Rev. B.**105**, 235422 (2022).
3. Mohanty, S., Deb, P. – Nontrivial band topology coupled thermoelectric in VSe2/MoSe2 van der Waals magnetic Weyl semimetal, J. Phys.: Condens. Matter **34**, 335801 (2022).
4. Bora, M., Deb, P. – Magnetic proximity effect in two-dimensional van der Waals heterostructure , J. Phys. Mater. **4**, 034014 (2022).
5. Behera, S. K., Bora, M., Chowdhury, S. S. P., Deb, P. – Proximity effects in graphene and ferromagnetic CrBr3 van der Waals heterostructure s, Phys. Chem. Chem. Phys. **21**, 25788-25796 (2019).
6. Behera, S. K., Deb, P. - PAW-mediated ab initio simulations on linear response phonon dynamics of anisotropic black phosphorous monolayer for thermoelectric applications, Phys. Chem. Chem. Phys. **20**, 26688-26695 (2018).
7. Bora, M., Deb, P. – Proximity induced longitudinal and transverse thermoelectric response in graphene-ferromagnetic $CrBr_3$ vdW

heterostructure , J. Phys.: Condens. Matter (2022). DOI: 10.1088/1361-648X/aca3e9.

8. Behera, S. K., Deb, P. – Spin-transfer-torque mediated quantum magneto transport in MoS2/Phosphorene vdW heterostructure based MTJs, Phys. Chem. Chem. Phys. **22**, 19139-19146 (2020).

9. Pham, T. A., Govoni, M., Seidel, R., Bradforth, S. E., Schwegler. E., Galli, G. - Electronic structure of aqueous solutions: Bridging thegap between theory and experiments, Sci. Adv. **3**, e1603210 (2017).

10. Pradhan, S. S., Konwar, K., Ghosh, T. N., Mondal, B., Sarkar, S. K., Deb, P. - Multifunctional Iron oxide embedded reduced graphene oxide as a versatile adsorbent candidate for effectual arsenic and dye removal, Colloids Interface Sci. Commun. **39**, 100319 (2020).

11. Talukdar, M., Behera, S. K., Bhattacharya, K., Deb, P. – Surface modified mesoporous g-C3N4@FeNi3 as prompt and proficient magnetic adsorbent for crude oil recovery, Appl. Surf. Sci. **473**, 275-281 (2018).

12. Talukdar, M., Behera, S. K., Deb, P. – Graphitic carbon nitride decorated with FeNi3 nanoparticles for flexible planar micro-super capacitor with ultrahigh energy density and quantum storage capacity, Dalton Trans. **48**, 12137-12146 (2019).

13. Talukdar, M., Nath, O., Deb, P. – Enhancing barrier properties of biodegradable film by reinforcing with 2D heterostructure , Appl. Surf. Sci. **541**, 148464 (2021).

14. Talukdar, M., Deb, P. – Recent progress in research on multifunctional graphitic carbon nitride: An emerging wonder material beyond catalyst, Carbon **192**, 308-331 (2022).

15. Sharma, M., Talukdar, M., Deb, P. – High connectivity hierarchical porous network of polyurethane engineered by nano flakes for proficient oil recovery, Appl. Surf. Sci.**601**, 154210 (2022).

16. Castellanos-Gomez, A. – Why all the fuss about 2D semiconductors? Nat. Photon. **10**, 202-204 (2016).

17. Won, R. – Flat talk, Nat. Photon. 10, 205-206 (2016).

18. Neugebauer, J., Hickel, T. – Density functional theory in materials science, WIREs Comput. Mol. Sci. **3**, 438-448 (2013).

19. Becke, A. D. - Perspective: Fifty years of density-functional theory in chemical physics. J. Chem. Phys.**140**, 18A301 (2014).

20. Kohn, W., Becke, A. D., Parr, R. G. - Density Functional Theory of Electronic Structure. J. Phys. Chem.**100**, 12974 (1996).

21. Hohenberg, P., Kohn, W. - Inhomogeneous electron gas. Phys. Rev.**136**, B864-B871 (1964).

22. Kohn, W., Sham, L. J. - Self-consistent equations including exchange and correlation effects. Phys. Rev.**140**, A1133-A1138 (1965).

23. Bl*ö*chl, P. E. - Projector augmented-wave method. Phys. Rev. B**50**, 17953 (1994).

24. Perdew, J. P., Burke, K., Ernzerhof, M. - Generalized Gradient Approximation made simple. Phys. Rev. Lett.**77**, 3865 (1996).

25. Giannozzi, P., Baroni, S., Bonini, N., Calandra, M., Car, R., Cavazzoni, C., Ceresoli, D., Chiarotti, G. L., Cococcioni, M., Dabo, I., Corso, A. D., de Gironcoli, S., Fabris, S., Fratesi, G., Gebauer, R., Gerstmann, U., Gougoussis, C., Kokalj, A., Lazzeri, M., Martin-Samos, L., Marzari, N., Mauri, F., Mazzarello, R., Paolini, S., Pasquarello, A., Paulatto, L., Sbraccia, C., Scandolo, S., Sclauzero, G., Seitsonen, A. P., Smogunov, A., Umari, P., Wentzcovitch, R. M. - QUANTUM ESPRESSO: a modular and open-source software project for quantum simulations of materials. J. Phys.: Condens. Matter, **21**, 395502 (2009).

26. Sahni, V., Bohnen, K. -P., Harbola, M. K., Analysis of the local-density approximation of density-functional theory, Phys. Rev. A**37**, 1895 (1988).

27. Björkman, T., Gulans, A., Krasheninnikov, A., Nieminen, R. - Are we van der Waals ready? J. Phys.:Condens. Matter,**24**,424218 (2012).

28. Fermi, E.- Un metodostatistico per la determinazione di alcunepropriet dell' atomo. Rend. Accad. Naz. Lincei, **6**,602-607 (1927).

29. Thomas, L. H. - The calculation of atomic fields. Mathematical Proceedings of the Cambridge Philosophical Society, **23**, 542548 (1927).

30. Kaplan, T. A., Kleiner, W. H. - Hartree-Fock Theory: Slater determinants of Minimum energy. Phys. Rev.**156**, 1 (1967).

31. Rehn, D. A., Wills, J. M., Battelle, T. E., Mattsson, A. E. - Dirac's equation and its implications for density functional theory-based calculations of materials containing heavy elements. Phys. Rev. B,**101**, 085114 (2020).

32. Jones, W., Young, W. H. - Density functional theory and the von Weizsacker method. J. Phys. C: Solid State Phys.,**4**, 1322 (1971).

33. Slater, J. - The theory of complex spectra. Phys. Rev.,**34**, 1293 (1929).

34. Soler, J. M., Artacho, E., Gale, J. D., Garcia, A., Junquera, J., Ordejon, P., Sanchez-Portal, D. - The SIESTA method for *ab initio* order-materials simulation. J. Phys.: Condens. Matter, **14**, 2745-2779 (2002).

35. Hamann, D. R., Schluter, M., Chiang, C. - Norm-conserving pseudopotentials. Phys. Rev. Lett., **43**, 1494-1497 (1979).

36. Kleinman, L. and Bylander, D. M. Efficacious form for model pseudopotentials. Phys. Rev. Lett.,**48**, 1425-1428 (1982).

37. Laasonen, K., Pasquarello, A., Car, R., Lee, C., Vanderbilt, D. - Carparrinello molecular dynamics with vanderbilt ultrasoft pseudopotentials. Phys. Rev. B,**47**, 10142-10153 (1993).

38. Vanderbilt, D. Soft self-consistent pseudopotentials in a generalized eigenvalue formalism. Phys. Rev. B, **41**, 7892-7895 (1990).

39. Fan, M., Wu, J., Yuan, J., Deng, L., Zhong, N., He, L., Cui, J., Wang, Z., Behera, S. K., Zhang, C., Lai, J., Jawdat, B. I., Vajtai, R., Deb, P., Huang, Y., Qian, J., Yang, J., Tour, J. M., Lou, J., Chu, C. -W., Sun, D., Ajayan, P. M., - Doping nanoscale graphene domains improves magnetism in hexagonal boron nitride,Adv. Mater., **31**, 1805778 (2019).

40. Talukdar, M., Behera, S. K., Jana, S., Samal, P., Deb, P. - Band alignment at heterointerface with rapid charge transfer supporting excellent photocatalytic degradation of Methylene blue under sunlight, Adv. Mater. Interface, **9**, 2101943 (2022).

41. Choudhary, K., Kalish, I., Beams, R., Tavazza, F., - High-throughput identification and characterization of two-dimensional materials using density functional theory, Sci. Rep., **7**, 5179 (2017).

42. Perdew, J. P., Chevary, J. A., Vosko, S. H., Jackson, K. A., Pederson, M. R., Singh, D. J.,Fiolhais, C. - Atoms, molecules, solids, and surfaces: Applications of the generalized gradient approximation for exchange and correlation. Phys. Rev. B, **46**, 6671-6687 (1992).

43. Fabiano, E., Constantin, L. A., Sala, F. D. - Generalized gradient approximation bridging the rapidly and slowly varying density regimes: A PBE-like functional for hybrid interfaces, Phys. Rev. B, **82**, 113104 (2010).

44. Horton, M. K., Montoya, J. H., Liu, M., Persson, K. A. – High-throughput prediction of the ground-state collinear magnetic order of inorganic materials using Density functional theory, npj Comp. Mater., **5**, 64 (2019).

45. Ren, Y., Qiao, Z., Niu, Q. - Topological phases in two-dimensional materials: a review, Rep. Prog. Phys., **79**, 066501 (2016).

46. Dresselhaus, G. – Spin-orbit coupling effects in zinc blende structures, Phys. Rev., **100**, 580 (1955).

47. Bychkov, Y. A., Rashba, E. I. - Properties of a 2D electron gas with lifted spectral degeneracy, JETP Lett., **39**, 78 (1984).

48. Murakami, S., Nagaosa, N., Zhang, S. C. - Dissipationless Quantum Spin Current at Room Temperature, Science, **301**, 1348 (2003).

49. Hasan, M. Z., Kane, C. L., - Colloquium: Topological insulators, Rev. Mod. Phys., **82**, 3045 (2010).

50. Marzari, N., Mostofi, A.A., Yates, J.R., Souza, I. Vanderbilt D. - Maximally localized Wannier functions: Theory and applications,Rev. Mod. Phys., **84**, 1419–1475 (2012).

51. Webster, L., Yan, J. -A. - Strain-tunable magnetic anisotropy in monolayer CrCl3, CrBr3, and CrI3, Phys. Rev. B, **98**, 144411 (2018)

52. Song, H. D., Zhu, P. F., Yang, X., Qin, M., Ren, Z., Duan, C. G., Han, G., Liao, Z. M., Yu, D. – Electrical control of magnetic proximity effect in a graphene/multiferroic heterostructure, Appl. Phys. Lett., **113**, 183101 (2018).

53. Behera, S. K., Deb, P. - Controlling the bandgap in graphene/h-BN heterostructures to realize electron mobility for high performing FETs, RSC Adv., **7**, 31393 (2017).

54. Lee, Y. -K. – Density functional theory (DFT) calculations and catalysis, Catalysts, **11**, 454 (2021).

55. Norskov, J. K., Abild-Pedersen, F., Studt, F., Bilgaard, T. – Density functional theory in surface chemistry and catalysis, PNAS, **108**, 937-943 (2011).

56. Chizallet, C.,Raybaud, P. - Density functional theory simulations of complex catalytic materials in reactive environments: Beyondthe ideal surface at low coverage. Catal. Sci. Technol.,**4** 2797 (2014).

57. Chen, C., Kong, W. X., Zhang, J. - A first-principles study on CO2 adsorption of Al5Mg2-cluster, Journal of Xinjiang University, **32**, 326-329 (2015).

58. Sheppard, D., Xiao, P., Chemelewski, W., Johnson, D. D., Henkelman, G. – A generalized solid-state nudged elastic band method, J. Chem. Phys., **136**, 074103 (2012).

59. Li, H., Xiao, J., Fu, Q., Bao, X. – Confined catalysis under two-dimensional materials, PNAS, **114**, 5930 (2017).

60. Skfflason, E.,Tripkovic, V., Bjçrketun, M. E.,Gudmundsdottir, S., Karlberg,G.,Rossmeisl, J., Bligaard, T.,Jonsson, H.,Nørskov, J. K. – Modeling the electrochemical hydrogen oxidation and evolution reactions on the basis of density functional theory calculations,J. Phys. Chem. C **114**, 18182–18197 (2010).

61. Behera, S. K., Deb, P., Ghosh, A. – Mechanistic study on electrocatalytic hydrogen evolution by high efficiency graphene/MoS2 heterostructure, Chem. Select **2**, 3657 (2017).

INDIAN JOURNAL OF THEORETICAL PHYSICS, VOL 70, NOS. 1 & 2, 2022

Fiber Optic Communication

Asit K. Datta

Department of Applied Optics and Photonics

University of Calcutta

Email: asitdatta@gmail.com

[Abstract: This article gives an overview of various aspects of fiber optic communication technologies, starting from the evolution and structures of optical fiber, to the recent trends in networking and fiber-based communication technologies. Fiber optic communication is a method of transmitting information by sending pulses of infrared light through an optical fiber. Fiber is preferred over electrical cabling when high bandwidth, long distance, or immunity to electromagnetic interference is required. This type of communication can transmit voice, video, and telemetry through local area networks or across long distances. Recent advances in fiber optic communication are the technique of wavelength division multiplexing, where multiplexing multiple optical carrier signals through a single optical fiber channel occurs by varying the wavelengths of laser light. WDM allows communication in both directions in a single optical fiber. Another useful development in fiber optics technology is doped fiber amplifiers that use doped optical fiber as a gain medium to amplify an optical signal. Amplification is achieved by stimulated emission of photons from dopant ions, such as erbium in the doped fiber.]

Keywords: Optical fiber, Optical communication, Wavelength division multiplexing, Doped optical fiber.

1. Information communication

A restricted framework for discussion has to be set when one presents an overview of the technologies of communication using optical fiber, properly indicating the usefulness of the techniques in comparison with the existing electronic counterparts. Moreover the priorities and utilities have to be assessed in view of the information explosions and exploitation which has been taking place at a breathtaking pace.

We have now entered into the information society: a society in which the very existence of its member is intimately dependent on the ability to harness the information for the betterment of services and business. Information transmission, processing, and storage are innate components of the information age. These activities are closely related with the terms ‘data’, ‘information’ and ‘knowledge’. An artificially constrained meaning of these words is necessary.

The word information was most probably derived from the Latin verb *informare* (to inform), which in turn may have derived from a French word informer, meaning a quantity to give form, or to form an idea of. During the fag end of the last century, the term information was defined as knowledge that can be transmitted without loss of integrity, thus suggesting that information is one form of knowledge. In the same sense, knowledge was identified as a state of preparedness built up partly by personal commitment, interests, and experiences and partly by the legacy of the tradition of the society. Knowledge is therefore fundamentally tacit.

At the outset, it is necessary to distinguish between the three words, data, information, and knowledge. In everyday discourse, the distinction between data and information, on the one hand, and between information and knowledge, on the other, remains typically vague. The terms data and

information are used interchangeably and the notion of information is conflated with knowledge. Fundamentally, data are sensory stimuli that are perceived through our senses. Information is that subset of data that has been processed into a meaningful form for a user. Knowledge is what has been understood and evaluated by the user. The following three points summarize the essential differences between the three words and concepts

1. DATA : Data are syntactic entities with no meaning; they are input to an interpretation process i.e. to the initial step of decision making.
2. INFORMATION : Information is interpreted data. It is the output from data interpretation as well as the input to, and output from, the knowledge-based process of decision making.
3. KNOWLEDGE : Knowledge is learned information incorporated in the user's reasoning resources, and made ready for active use within a decision process; it is the output of a learning process.

Therefore, the data is information when used in decision-making, but goes beyond this definition since it links the use of data to the underlying interpretation process that enables its use. Knowledge, then, is what is needed in order to perform the interpretation and what gets learned from new information. The role of knowledge, in general, is therefore to play an active part in the processes of transforming data into information, deriving other information, and acquiring new knowledge. The following process gives the route to transforming data into knowledge.

1. Transform data into information - referred to as data interpretation
2. Derive new information from existing - referred to as elaboration
3. Acquire new knowledge - referred to as learning .

This introduction sets the stage for the impact analysis of the fiber optic techniques of communication. Today's environment is different from the earlier industrial age. The overall volume of commercial and entertainment activities has increased. Apparently, more of these increases occur in the service sector as information transmission, processing, and storage facilities followed by the dissemination of knowledge as defined.

Fiber optics technology or in the broader term optical communication technology with its ability to improve information related transaction is playing an increasingly dominant role in shaping this environment. Major theoretical development in the area of information communication process started with Shannon's classical theorems on code capacity and channel capacity. Shannon's ideas have been crucial in enabling the advances in information and communication technology. In fact, his works were referred to as the Magna Carta of the information age. However, Shannon's theorems did not provide the methods for achieving ideal channel capacity for a given statistics of the channel, with which all practical communication systems can be evaluated with respect of their efficiency. Shannon's theory showed how to design more efficient information communication and storage systems by demonstrating the enormous gains achievable by coding, and by providing the intuition for the correct design of coding systems. While developing the theorems and subsequent theories related to various aspects of information, the question of the uncertainty of information either generated or received have become an important issue.

Two important aspects of information communication are the speed and the bandwidth. Communication speed is the maximum transfer rate of information over a channel. Essentially, it is a measure of how fast data can be sent over a wired or wireless channel and is usually measured in bits per second.

Bandwidth is a range of frequencies within a continuous set of frequencies. It is a key concept in many information communication applications. In radio communications, for example, bandwidth is the frequency range occupied by a modulated carrier signal, where signals do not mutually interfere or attenuated. Another definition of bandwidth for a system or communication links could be the range of frequencies over which the system produces a specified level of performance. A less strict and more practically useful definition refers to the frequencies beyond which performance is degraded.

A very naïve example may be given to explain the terms, speed and bandwidth in the context of information communication. Suppose that a man riding a horse is carrying some information from one place to another. Then the speed of information communication is the speed at which a horse can run. At a gallop a horse can run at an average speed of say 60 km per hour. So the speed of information transmission is about 16 m per second. Now suppose ten such horse riders are carrying information from one point to another *side by side* through a path ways (channel) without any hindrance. So the bandwidth is the width of the pathways. Now if, 15 horse riders are pushed through the same pathways, there is every chance of collision and hence loss of information. So the pathway (or bandwidth) is not sufficient for carrying information and the channel is now band-limited. Fiber optic cables have a much larger bandwidth of over 60 Tbps in comparison to 10 Gbps bandwidth of copper wires.

1.1 Why communication using optical fiber is better?

We are all familiar with the fact that TV transmission utilizes VHF/UHF waveband (30-30000 MHz) while normal radio broadcast utilizes lower frequencies (300 KHz to 30 MHz) of the electromagnetic

spectrum. The reason for this is that the information content of the TV signals cannot be sent intelligently without loss of information using radio frequencies as a carrier. Indeed, the higher one goes up in the electromagnetic spectrum in frequency scale, the higher would be the information-carrying capacity of a communication system. Since the optical beams have the frequencies in the range of 10^{14} -10^{15} Hz, the use of such beams as a carrier would imply a tremendously large increase in the information transmission capacity of the system. However, a light beam (even a laser beam) carrying signals cannot be sent in an open atmosphere over a long distance because of severe attenuation and distortion due to absorption and scattering by the atmosphere. Therefore a better media that is, the optical fiber has been developed for carrying light beams, with small attenuation and dispersion.

The advantages of an optical fiber communication system are:

1. Higher bandwidth of transmission: Whereas the allowable bandwidth in copper cables are nearly 500 MHz and 700 MHz in radio systems, optical fiber based communication systems provide a potential bandwidth in the order of GHz, since the optical carrier frequency ranges between 10^{13} to 10^{16} Hz. Thus with higher bandwidth and low-loss characteristic, fibers have a higher information-carrying capacity.
2. No cross-talk or interference: Since optical fibers are dielectric waveguides, they are free from electromagnetic interference (EMI) and require no EMI shielding. Hence data communication in an optical fiber is unaffected in an electrically noisy environment.
3. Low loss: In comparison to copper cables, fibers exhibit very low attenuation (less than 0.2dB/km) or transmission loss. Hence fiber

communication systems have wide repeater amplifier spacing, thus reducing system cost and complexity.

4. Security: Unlike metallic-based systems, the dielectric nature of optical fiber makes it impossible to remotely detect the signal being transmitted within the cable. Accessing the fiber requires intervention that is easily detectable by security surveillance. These issues make fiber extremely attractive to banking and other sensitive information communication systems.
5. Small size, lightweight and low cost: Owing to the core diameter being very small, the optical fiber is lightweight as compared to copper wire. Again, when compared to copper based wires and cables optical fiber and optical fiber cables are of lower cost.
6. Ruggedness and system reliability: The optical fiber is rugged and can withstand high temperatures and is of high tensile strength.

2 History of optical fiber development

In 1954 Harold Hopkins and Narinder Singh Kapany showed that rolled fiberglass allowed light to be transmitted. Jun-ichi Nishizawa, a Japanese scientist at Tohoku University, proposed the use of optical fibers for communications in 1963. In 1966 Charles K. Kao and George Hockham at Standard Telecommunication Laboratories showed that the losses of 1,000 dB/km in existing glass (compared to 5-10 dB/km in coaxial cable) were due to contaminants that could potentially be removed.

Optical fiber with attenuation low enough for communication purposes (about 20 dB/km) was developed in 1970 by Corning Glass Works. After a period of research starting in 1975, the first commercial fiber-optic telecommunications system was developed which operated at a wavelength of around 0.8 μm and used GaAs semiconductor lasers. This

first-generation system operated at a bit rate of 45 Mbit/s with repeater spacing of up to 10 km. Soon in 1977, General Telephone and Electronics sent the first live telephone traffic through fiber optics at a 6 Mbit/s throughput.

The second generation of fiber-optic communication was developed for commercial use in the early 1980s, operated at 1.3 μm and used InGaAsP semiconductor lasers. These early systems were initially limited by multi-mode fiber dispersion, and in 1981 the single-mode fiber was revealed to greatly improve system performance. By 1987, these systems were operating at bit rates of up to 1.7 Gbit/s with repeater spacing of up to 50 km. Third-generation fiber-optic systems operated at 1.55 μm and had losses of about 0.2 dB/km, eventually allowing systems to operate commercially at 2.5 Gbit/s with repeater spacing move than 100 km.

By 1996, the fourth generation of fiber-optic communication systems came into the market using optical amplification to reduce the need for repeaters and wavelength-division multiplexing (WDM) to increase data capacity. The introduction of WDM was the start of optical networking, as WDM became the technology of choice for fiber-optic bandwidth expansion. The introduction of optical amplifiers and WDM caused system capacity to double every six months from 1992 until a bit rate of 10 Tb/s was reached by 2001. In 2006 a bit-rate of 14 Tb/s was reached over a single 160 km line using optical amplifiers. As of 2021, Japanese scientists transmitted 319 terabits per second over 3,000 kilometers with four-core fiber cables with standard cable diameter.

The focus of development for the fifth generation of fiber-optic communications are on extending the wavelength range over which a WDM system can operate. The conventional wavelength window, known as the C

band, covers the wavelength range 1525-1565 nm, and dry fiber has a low-loss window promising an extension of that range to 1300-1650 nm. Other developments include the concept of optical solitons, pulses that preserve their shape by counteracting the effects of dispersion with the nonlinear effects of the fiber by using pulses of a specific shape. In 2022, Technical University of Denmark reported a system operating at 1.84 Pbit/s in a 37 channel optical fiber each operating at 223 Gbit/s over a length of 7.9 km.

3 Light propagation in optical fiber

The modern impetus in information communication with carrier waves at optical frequencies owes its origin to the invention and practical realization of lasers and optical fibers. As a result, today optical communication is the most useful and advanced mode of information communication technology, fueled by the ever-increasing demands of higher bandwidth. This increasing trend, of the need for large bandwidths, even continues today. Optical fiber communication systems operate in the frequency spectrum (frequencies between 10^{13} Hz to 10^{15} Hz).

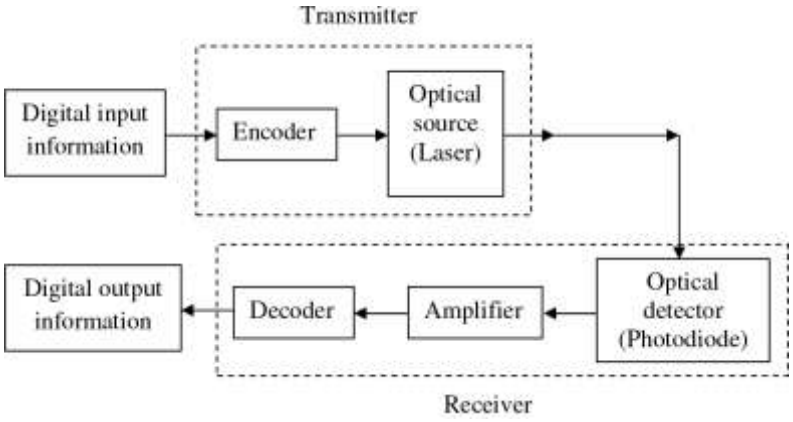

Fig. 1: Fiber optic communication system.

Like any other communication system, optical communication systems operate on the same concept as other wired communication systems

as shown in Figure.1. This too has three basic modules transmitter, receiver, and the channel or medium of communication. The input information is encoded and accordingly transmitted as a modulated optical signal through the optical fiber by an optical source at one end and detected by a detector at the other end of the fiber. Encoding, multiplexing, and other electronic circuits are necessary for converting information into the optical signal form at the transmitter. The detected optical signal is amplified and then decoded to obtain the output information. All electronic circuits necessary to decode, demultiplex along with the detector and associated amplifier form the receiver. The optical source serves as the electrical to optical signal converter, which may be either a light emitting diode (LED) or preferably a semiconductor laser. The detector is a photodiode (e.g. P-I-N diode or Avalanche photodiode) that converts the optical signal back to electrical signal.

4 Optical fiber

Optical fibers are concentric cylindrical waveguides made of an internal core and a surrounding clad layer. The core with refractive index n_1 serves as the medium for light propagation, while the cladding has a lower refractive index n_2 where $n_1 > n_2$. When a light ray encounters the interface of a fiber, the light ray is refracted and its direction of propagation changes according to Snell's law of refraction, such that light rays are reflected back to the core.

The basic phenomenon of guidance can be explained by ray model of optical fiber. Guiding of light is through the total internal reflection, i.e., only rays with incident angle greater than the critical angle, at the clad-core interface, are transmitted, as shown in Figure.2. The maximum angle of incidence at which the light is launched into the fiber and gets propagated

inside the fiber is thus given by $(\phi_i)_{max}$ and is also called the acceptance angle. The cone formed by the acceptance angle is called the acceptance cone. Rays greater than the acceptance angle may enter the core but are refracted to the cladding and eventually lost by radiation.

Considering the refractive index of air to be unity, using Snell's law for at the air-core interface, as seen in Figure.2

$$\sin \phi_i = n_1 \sin \phi_r \quad \ldots (1)$$

where ϕ_r is the angle of refraction at the air-core interface. From the Figure.2, it is obvious that $\phi_r = \left(\frac{\pi}{2}\right) - \theta$. Again for angles larger than the critical angle θ at the core-clad interface given by

$$n_1 \sin \theta = n_2 \quad \ldots (2)$$

For confining rays within fiber core, this necessary condition has to be obeyed. Thus eq.1 becomes

$$\sin \phi_i = n_1 \sin\left(\left(\frac{\pi}{2}\right) - \theta\right)$$

$$= n_1 \cos \theta$$

$$= n_1\sqrt{(1 - \sin^2 \theta)} \quad \ldots (3)$$

$$= n_1 \sqrt{\left(1 - \frac{n_2^2}{n_1^2}\right)}$$

where n_1 and n_2 are the refractive index of the core and clad respectively.

The acceptance angle or the maximum angle of incidence (ϕ_i) is related to the refractive indices by

$$(\phi_i)_{max} = \sqrt{n_1^2 - n_2^2} \quad \ldots (4)$$

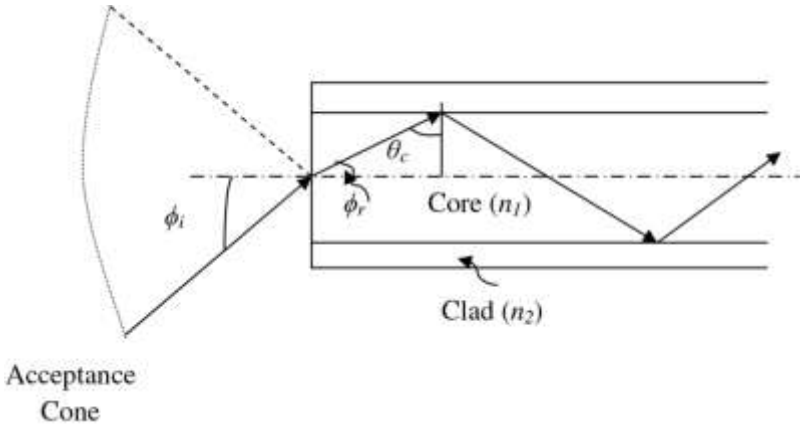

Fig. 2: Launching of light and its propagation inside the fiber.

An important fiber parameter is the numerical aperture (NA) which is simply equal to $\sin(\phi_i)_{max}$. Thus

$$NA = (\phi_i)_{max} = \sqrt{n_1^2 - n_2^2} \quad \ldots (5)$$

NA represents the light gathering capacity of the optical fiber.

For propagation of light inside the core there are possibilities that the light may get transmitted as *meridional rays* or as *skew rays*. When a light ray is launched in a plane containing the axis of the fiber, the light ray after total internal reflection travels in the same plane in which it was launched. Thus the ray will always cross the axis of the fiber while propagating and is hence called the *meridional rays*. Whereas, when the ray is not launched in a plane containing the axis of the fiber, i.e., launched at some angle not intersecting the axis of the fiber, then after total internal reflection the ray will never intersect the axis of the fiber. The ray essentially will spiral around the axis of the fiber and is thus called the *skew rays.*

As mentioned earlier, when the angle of incidence at the core and clad interface $\theta_{inter\,face}$ is greater than the critical angle θ, a ray propagates through the optical fiber. So rays having $\theta \geq \theta_{inter\,face} \leq \pi/2$ will

propagate along the fiber with some discrete velocities, known as modal velocities. The interference of the traveling waves inside the fiber gives rise to different modes within the fiber. A specific mode is obtained only when the angle between the rays and the core-clad interface has a particular value. Modes can therefore be termed as the stable electric field distributions within the fiber core.

Modes in an optical fiber can be expressed by the wave theory and principles of the waveguide. Treating light as a transverse electromagnetic wave, during the propagation of *meridional rays* along the fiber, the electric and magnetic fields of all the rays superimpose to result in electric and magnetic field distribution which may be either transverse electric TE_x or transverse magnetic TM_x in nature. The subscript x denotes the definite number of maxima and minima in the resultant light intensity pattern. The propagation of skew rays, on the other hand, results in a particularly special form of modes which are neither TE nor TM in nature and are called hybrid modes. Figure. 3 shows different intensity patterns created by the superposition of the wave fronts of all the light rays for transverse electric modes that propagate in an optical fiber. The fields that are shown in the cladding region are actually the evanescent fields that exist in the cladding owing to the boundary condition requirement at the core-cladding interface. For very low launching angles with respect to the axis of the fiber, the intensity pattern created is the one which is shown as TE_0 in the figure. There exists a maximum intensity region around the axis of the core and the fields start to decay towards the periphery of the core. These fields eventually decay down to negligibly low values in the cladding. If the launching angle is increased further, the intensity patterns are shown for

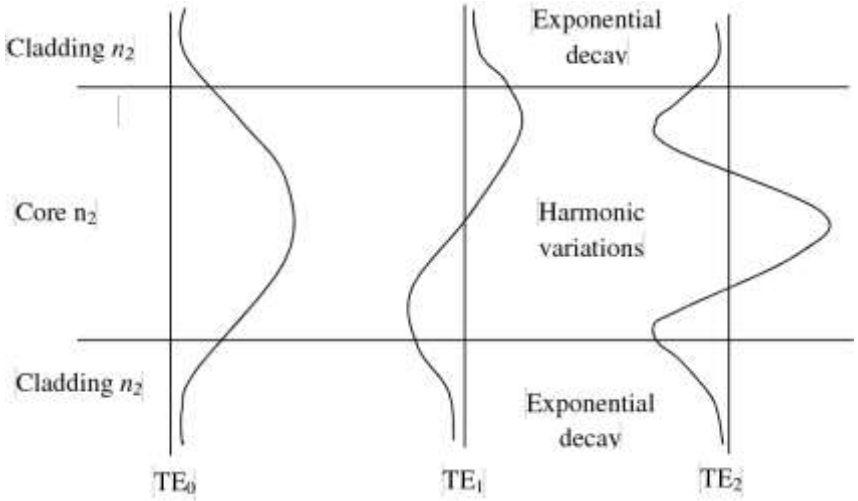

Fig. 3: Different TE modes in an optical fiber

TE_1 and TE_2 in the above figure. The subscript of TE in fact indicates the number of destructive interferences in the pattern where the field intensity crosses the zero level, or in other words, creates an optically dark area. So, no dark area exists for TE_0. For TE_1 and TE_2 one and two dark areas are possible and for higher TE modes more dark areas are possible.

The ray model of light showed that the launching angle of the light ray must be smaller than the acceptance angle of the optical fiber core. But the consideration of the wave fronts establishes that this condition of the launching angle is not enough to ensure a successful propagation of light in an optical fiber. The launching angle must be such that the angle of refraction of the launched ray into the fiber must satisfy the phase condition of the equation given below for sustained propagation inside the optical fiber core.

$$\frac{2\pi n_1 \, d \sin\theta}{\lambda} + \delta = \pi m \qquad \ldots (6)$$

where $m = 1, 2, 3\ldots, n_1$ is refractive index of core, λ is the Wavelength of the light in the core, d is the diameter of the core and δ is the phase change undergone in each total internal reflection of a ray.

The different discrete values of the angle θ indirectly signify the different allowable launching angles of the light rays into the optical fiber. For $m = 0$, in the above equation leads to $\theta = 0$. This refers to the ray that propagates along the axis and it does not require any phase condition to be satisfied. Taking the value of $m = 1$, the value of θ for first order mode is

$$\theta_1 = \sin^{-1}\left[\frac{\lambda(\pi - \delta)}{2\pi d n_1}\right] \quad \ldots (7)$$

The value of θ_1 signifies the first annular ring of rays that propagates inside the fiber. Similarly, the other modes that propagate in the fiber by subsequent substitution of the corresponding values of m is obtained until the condition $\theta \leq \alpha$ is reached, where α is the numerical aperture of the fiber core.

4.1 Types of optical fiber

Fibers are classified as *step-index* (SI) or *graded index* (GI) fibers depending on the refractive index profile of the core, as shown in Figure.4. Step-index fibers have a core of uniform refractive index profile and the profile is expressed as

$$n(r) = \begin{cases} n_1 \text{ if } r < a \\ n_2 \text{ if r} \geq \text{a} \end{cases} \quad \ldots (8)$$

However, depending on the modes of propagation, the step-index fibers may be single-mode or multi-mode fibers. The term multimode refers to the fact that multiple modes or light paths through the fiber are possible. The number of modes (V) supported in a fiber is determined by the

refractive index, operating wavelength and the diameter of the core. Single-mode step index fiber allows only one path, or mode, for light to travel within the fiber. In a multimode step-index fiber, the number of modes M_n propagating can be approximated expressed as

$$M_n = \frac{V^2}{2} \qquad \ldots (9)$$

where, V is known as the normalized frequency, or the V-number and is given by

$$V = 2\frac{\pi a}{\lambda}\sqrt{n_1^2 - n_2^2} \qquad \ldots (10)$$

$$= 2\frac{\pi a}{\lambda}(NA)$$

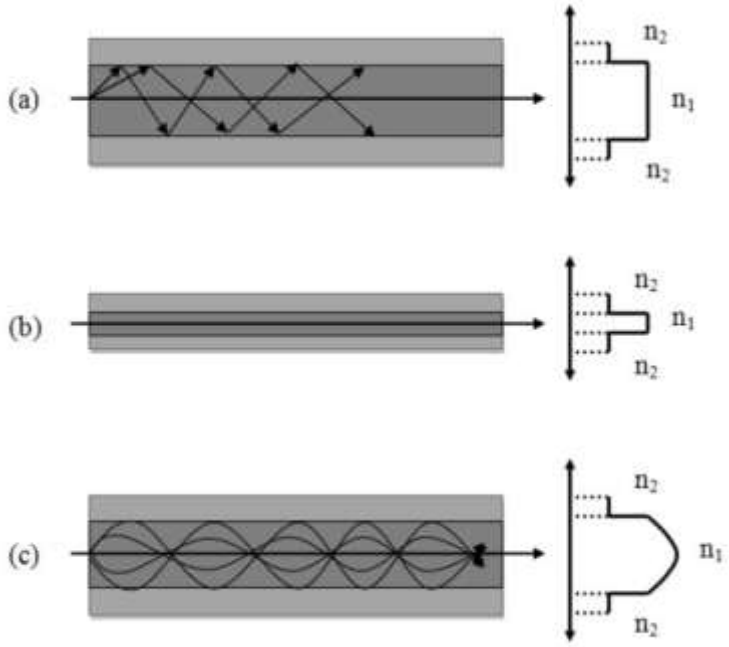

Fig. 4: Types of Fiber with their profiles and ray-paths within the fiber: (a) Multi-mode Step-index (b) Single-mode Step-index and (c) Graded index.

where a is the core diameter. From the equation, it is seen that reducing the core-radius reduces the possible number of modes V passing through the fiber. The total number of guided modes M for multi-mode fibres is $M = 0.5V^2$ for multi-mode silicon fiber and $M \approx 0.25V^2$ for multi-mode germanium doped fiber. The analysis of how the V-number is derived is beyond the scope of this article, but it can be shown that by reducing the diameter of the fiber to a point at which the V-number is less than 2.405, higher-order modes are effectively extinguished and single-mode operation is possible.

The graded-index fiber or gradient-index fiber has a core that has a refractive index that decreases with increasing radial distance from the optical axis of the fiber. Hence light rays follow sinusoidal paths along the fiber length. The refractive index profile for a graded-index fiber is nearly parabolic and this parabolic profile result in continual refocusing of the rays in the core, thus minimizing modal dispersion. Graded-index fiber is characterized by its ease of use (i.e., large core diameter and NA.), similar to a step-index multimode fiber, and its greater information carrying capacity, as in a step-index single mode fiber. Light traveling through the center of the fiber experiences a higher index of refraction than does light traveling in higher modes. This means that even though the higher-order modes must travel farther than the lower order modes, they travel faster, thus decreasing the amount of modal dispersion and increasing the bandwidth of the fiber.

Fibers are represented by their core-cladding diameter as $2a/2b$, e.g., $8/125\ \mu m$ for single-mode step-index fiber and $62.5/125\ \mu m$ for multi-mode step index fibers, where a and b are the radii of core and cladding respectively. The base material for optical fibers is pure silica (SiO_2) in the

form of fused quartz (amorphous). The refractive index of the base material can be modified by the addition of impurities. For lowering refractive index, B_2O_3 or F can be used, whereas for increasing the refractive index, P_2O_5 or GeO_2 can be used. As already mentioned in this section, the cladding has a lower R.I. than the core of the fiber.

4.2 Signal distortion in optical fiber

When an optical signal is transmitted on an optical fiber, the signal is distorted owing to two phenomena. These phenomena are known as dispersion and attenuation. The following diagram shows the constituents of each phenomenon that contribute to the distortion of optical signal in the optical fiber.

(a) Dispersion: In optical communication systems, information to be sent is first coded in the form of light pulses and then transmitted from the transmitter to the receiver, where the information is decoded. The larger the number of pulses that can be sent per unit time and still be resolvable at the receiver end, the larger will be the transmission capacity, or bandwidth of the system. A pulse of light sent into a fiber broadens as it propagates through the fiber. This phenomenon is known as dispersion. Dispersion, expressed in terms of the symbol Δt, is defined as pulse spreading in an optical fiber. As a pulse of light propagates through a fiber, the numerical aperture or core diameter or refractive index profile or wavelength causes the input pulse to broaden, which in turn poses a limitation on the overall bandwidth of the fiber. Dispersion Δt can be determined as

$$\Delta t = \sqrt{\Delta t_{out} - \Delta t_{in}} \quad \text{... (11)}$$

where Δt_{out} and Δt_{in} are the output and input pulse widths through the fiber as shown in Figure.5. The dispersion is also a function of fiber length. The

overall effect of dispersion on the performance of a fiber optic system is

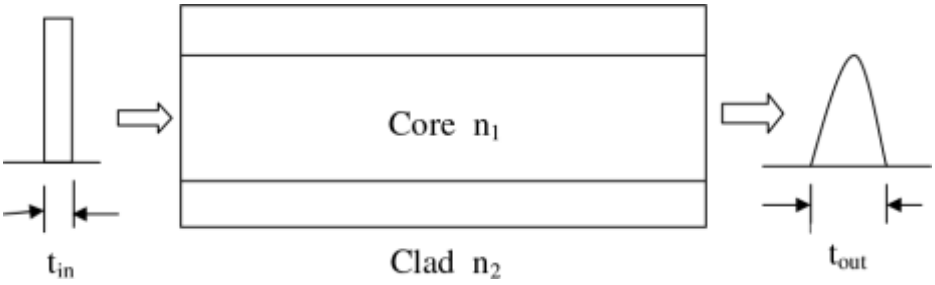

Fig. 5: Pulse broadening due to dispersion in a fiber.

known as inter symbol interference, which occurs when the pulse spreading due to dispersion causes the output pulses of a system to overlap, rendering them undetectable. If an input pulse is caused to spread such that the rate of change of the input exceeds the dispersion limit of the fiber, the output data will become indiscernible.

As seen in the diagram, different subcomponents of dispersion added together to form the total dispersion of an optical fiber of a certain length. These are: *Intermodal dispersion:* Intermodal dispersion is the pulse spreading caused by the time delay between lower-order modes (modes or rays propagating straight through the fiber close to the optical axis) and higher-order modes (modes propagating at steeper angles). Modal dispersion is the primary cause of bandwidth limitation in multimode fiber and it is not detrimental in single-mode fiber where only one mode is allowed to propagate.

Chromatic dispersion: Chromatic dispersion is pulse spreading due to the fact that different wavelengths of light propagate at slightly different speeds through the fiber. All light sources have finite line widths and therefore, they emit more than one wavelength. Because the index of refraction of glass fiber is a function of wavelength, different wavelengths propagate at different speeds. This contributes to the effect of chromatic

dispersion which is typically expressed in units of nanoseconds or picoseconds per km. Chromatic dispersion again consists of two parts: material dispersion and waveguide dispersion. Material dispersion is due to the wavelength dependency on the index of refraction of glass. Waveguide dispersion is due to the physical structure of the waveguide. Material dispersion and waveguide dispersion can have opposite signs (or slopes) depending on the transmission wavelength.

In the case of a step-index single-mode fiber, these two effects cancel each other at 1310 nm yielding zero-dispersion, which makes high-bandwidth communication possible at this wavelength. Because of the mismatch between minimum attenuation at 1550 nm and zero dispersion at 1310 nm, special zero-dispersion-shifted fibers are evolved. Zero-dispersion-shifted fiber shifts the zero dispersion wavelength of 1310 nm to coincide with the 1550 nm transmission window of glass fiber by modifying the waveguide dispersion slope. The modification is accomplished by modifying the refractive index profile of the fiber in a way that yields a more negative waveguide-dispersion slope. When combined with a positive material dispersion slope, the point at which the sum of two slopes cancels each other out can be shifted to a higher wavelength such as 1550 nm or beyond.

The total dispersion of an optical fiber, Δt_{tot}, can be approximated using

$$\Delta t_{tot} = [\Delta t_{modoel}^2 + \Delta t_{crom}^2]^{\frac{1}{2}} \quad \ldots (12)$$

The transmission capacity of fiber is typically expressed in terms of bandwidth × distance. For example, the (bandwidth × distance) product for a typical 62.5/125- (core/cladding diameter) multimode fiber operating at 1310 nm might be expressed as 600 MHz · km. The approximate

bandwidth BW of a fiber can be related to the total dispersion by the relationship, $BW(Hz) = 0.35/\Delta t_{tot}$.

(b) Attenuation: The phenomena of attenuation in optical fiber is another phenomenon that cause signal distortion in optical fiber. Moreover, fiber attenuation dictates the selection of transmission wavelength of an optical fiber communication system. Typical optical transmission wavelengths are 850 nm, 1310 nm, and 1550 nm. Figure. 6 shows the spectral dependence of fiber attenuation (i.e., dB loss per unit length) as a function of wavelength of a typical silica optical fiber. The losses are caused by various mechanisms such as Rayleigh scattering, absorption due to metallic impurities, OH ions in the fiber, and intrinsic absorption by the silica molecule itself. The Rayleigh scattering loss varies as λ^{-4}, i.e., longer wavelengths scatter less than shorter wavelengths. Rayleigh scatter causes the dB loss/km to decrease gradually as

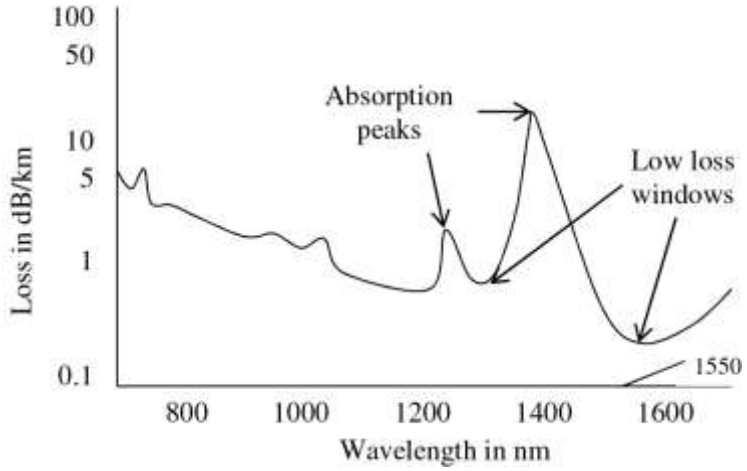

Fig. 6: Attenuation in optical fiber at different wavelength

the wave length increases from 800 nm to 1550 nm. The two absorption peaks around 1240 nm and 1380 nm are primarily due to traces of OH ions and metallic ions in the fiber which may be induced during the

manufacturing process. The level of purity required to achieve low-loss optical fibers is therefore very stringent. If these impurities are removed, the two absorption peaks will disappear. For $\lambda > 1600$ nm, the increase in the dB/km loss is due to the absorption of infrared light by silica molecules. This is an intrinsic property of silica, so no amount of purification can remove this infrared absorption tail. There are two windows at which the dB/km loss attains its minimum value. The first window is around 1300 nm (with a typical loss coefficient of less than 1 dB/km) where fortunately, the material dispersion is negligible. However, the loss coefficient is at its absolute minimum value of about 0.2 dB/km around 1550 nm. The latter window has become extremely important in view of the availability of erbium-doped fiber amplifiers.

For an optical fiber of length L (in kilometre), if P_{in} and P_{out} are the input and output optical power respectively, then attenuation constant α of the fiber in dB/Km is

$$\alpha = \frac{10}{L}\log_{10}\frac{P_{in}}{P_{out}} \quad \ldots(13)$$

5 Point to point fiber optic link

The so called point-to-point fiber link is the basic building block of any fiber optic communication system. Most generic point-to-point communication link consists of two endpoints connected by a link. In a generic configuration, an endpoint system could be a computer or terminal, either in an isolated location or physically connected to a network. The term communications link refers to the hardware and software connecting the nodes of a network. The role of the link is to transport information, available in the form of a digital bit stream, very accurately from one point of the network to another point. For short-haul or short-distance

communication, the link length may be less than a km, whereas, for long-haul or long-distance links, the link length may be thousands of km.

Figure.7 illustrates the concept. Loss of signal becomes a matter of concern, when the link length exceeds a certain value, say 200/100 km depending on the operating wavelength. Hence it becomes necessary to compensate for the fiber losses through the use of signal amplifiers or repeaters/regenerators at regular intervals along the length of the links. A regenerator consists of a receiver followed by a transmitter.

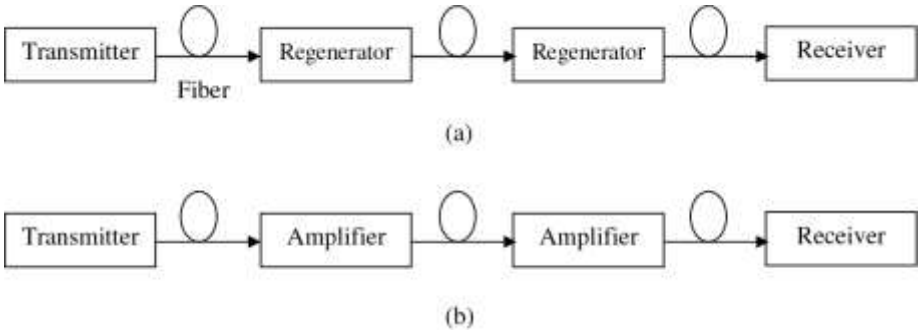

Fig. 7: Point-to-point fiber links with periodic loss compensation using (a) regenerators and (b) optical amplifiers.

Modern fiber-optic communication systems generally include optical transmitters that convert electrical signals into optical signals, optical fiber cables to carry the signal, optical amplifiers, and optical receivers to convert the signal back into an electrical signal. The information transmitted is typically digital information generated by computers or telephone systems.

5.1 Transmitters

A transmitter is an electrical-to-optical converter. The most commonly used optical transmitters are semiconductor devices such as light emitting diodes (LEDs) and laser diodes. The difference between LEDs and laser diodes that LEDs produce incoherent light, while laser diodes produce

coherent light. For use in optical communications, semiconductor optical transmitters must be designed to be compact, efficient, and reliable, while operating in an optimal wavelength range and directly modulated at high frequencies.

In its simplest form, an LED emits light through spontaneous emission, a phenomenon referred to as electroluminescence. The emitted light is incoherent with a relatively wide spectral width of 30 to 60 nm. The large spectrum width of LEDs is subject to higher fiber dispersion, considerably limiting their bit rate-distance product (a common measure of usefulness). LEDs are suitable primarily for local-area-network applications with bit rates of 10 to 100 Mbit/s and transmission distances of a few kilometers.

LED light transmission is inefficient, with only about 1% of the input power, or about 100 microwatts, eventually converted into launched power coupled into the optical fiber. LEDs have been developed that use several quantum wells to emit light at different wavelengths over a broad spectrum and are currently in use for local-area wavelength-division multiplexing (WDM) applications.

LEDs have been largely superseded by vertical-cavity surface-emitting laser (VCSEL) devices, which offer improved speed, power, and spectral properties, at a similar cost. However, due to their relatively simple design, LEDs are very useful for very low-cost applications. Commonly used classes of semiconductor laser transmitters used in fiber optics include VCSEL.

A semiconductor laser emits light through stimulated emission rather than spontaneous emission, which results in high output power (100 mW) as well as other benefits related to the nature of coherent light. The output of a

laser is relatively directional, allowing high coupling efficiency (50%) into single mode fiber. Common VCSEL devices also couple well to multimode fiber. The narrow spectral width also allows for high bit rates since it reduces the effect of chromatic dispersion. Furthermore, semiconductor lasers can be modulated directly at high frequencies because of the short recombination time.

Laser diodes are often directly modulated, that is the light output is controlled by a current applied directly to the device. For very high data rates or very long distance links, a laser source may be operated continuously wave, and the light modulated by an external device, an optical modulator, such as an electro-absorption modulator. For very high bandwidth efficiency, coherent modulation can be used to vary the phase of the light in addition to the amplitude.

5.2 Receivers

The main component of an optical receiver is a photodetector which converts light into electricity using the photoelectric effect. The primary photodetectors for telecommunications are made from Indium gallium arsenide. The photodetector is typically a semiconductor-based photodiode. Several types of photodiodes include p-n photodiodes, p-i-n photodiodes, and avalanche photodiodes. Metal-semiconductor-metal (MSM) photodetectors are also used due to their suitability for circuit integration in regenerators and wavelength division multiplexers.

Since light may be attenuated and distorted while passing through the fiber, photodetectors are typically coupled with a trans-impedance amplifier and a limiting amplifier to produce a digital signal in the electrical domain recovered from the incoming optical signal. Further signal processing such

as clock recovery from data performed by a phase-locked loop may also be applied before the data is passed on.

6 Basic design criteria

The primary design criteria signify the most basic information parameters to be made available by the user to the designer for designing a reliable fiber optic link. The first important information to be specified by the user is the desired bit rate of data transmission. However, the dispersion in the optical fiber exerts a limitation on the maximum achievable and realizable data rate of transmission. The next intricate information to be provided for the design process is the length of the optical link to enable the designer to ascertain the position of the optical repeaters along the link for a satisfactory optical data link. Along with the primary design criteria, there are some additional parameters that facilitate better design and quality analysis of the optical link. These factors consist of the scheme of modulation, the system fidelity, cost, commercial availability, etc.

In optical link design problems, the power of the optical source and the optical receiver are generally expressed in dBm. The dB equivalent power of 1mW power is taken as the reference i.e. 0 dBm and the increasing powers are expressed in their equivalent dBm values by normalizing them with respect to 1mW and for every 10-fold increase in the actual power, increases the dBm equivalent power by 10. For a typical optical transmitter with a laser source, the output power normally ranges between 3 to 5 dBm. A typical optical receiver requires about 30 to 40 dBm of detectable power for a bit error rate (BER) of 10^{-9}.

6.1 Loss budget

Having fixed the transmitter output power, P_s and sensitivity of receiver, P_r, the maximum possible allowable loss that can occur is the difference between the transmitter and the received powers. The loss occurs in the different components connected in the system such as the connectors, splices, the optical fiber, and also in the system itself which is known as the system margin. Generally a system margin of about 6 dB is pre-set in practical systems. The total loss is the total of all the losses occurring in each of these components (calculated per unit length). Therefore maximum allowable loss, α_{max} in dB is ($P_s - P_r$) and α_{max} is given by,

$$\alpha_{max} = \alpha_{fiber} + \alpha_{connectors} + \alpha_{splices} + \alpha_{system} \quad \ldots (14)$$

The maximum possible length (L_{max}) of the optical fiber that can be used in the above design, without affecting the system BER, can then be determined as

$$L_{max} = \frac{\alpha_{fiber}}{loss/km} \quad \ldots (15)$$

6.2 Rise-time budget

The next step in the design of an optical link is the rise time budget calculations. The rise time of a system is the time taken by the system to attain 90% of the steady-state response of the system (from the initial state) to a particular input. The rise time of a system varies inversely with its bandwidth. Rise time analysis gives the effective bandwidth of the optical link. The system rise time t_{sys} is calculated as a root mean square value of the transmitter rise time t_{tx}, the receiver rise time t_{rx} and the rise time associated with the optical channel dispersion $D\beta_{\lambda}$, where D is the

dispersion parameter, β_λ is the spectral width of the optical source, and L is the length of the optical link. Therefore the rise-time budget is given by

$$t_{sys} = \left[t_{tx}^2 + D^{2\beta_\lambda^2} + t_{rx}^2\right]^{\frac{1}{2}} \quad \ldots (16)$$

For a satisfactory operation of the optical link, the system rise time should be less than or equal to 70% of the bit duration at the specified data rate.

6.3 Modulation format

The modulation format used in optical communication is mainly known as the return-to-zero (RZ) and non-return-to-zero (NRZ) formats. A simple variation of a two-level block code of $nBmB$ type is 1B2B. This code is commonly known as Manchester or biphase code and is also preferred. In the RZ format, each optical pulse representing bit 1 is shorter than the bit slot, and its amplitude returns to zero before the bit duration is over. In the NRZ format, the optical pulse remains on throughout the bit slot and its amplitude does not drop to zero between two or more successive 1 bits. As a result, pulse width varies depending on the bit pattern, whereas it remains the same in the case of the RZ format. An advantage of the NRZ format is that the bandwidth associated with the bit stream is smaller than that of the RZ format by about a factor of two simply because on-off transitions occur fewer times. In 1B2B code, there are never more than two consecutive identical symbols, and two symbols are transmitted for one information bit, giving 50% redundancy. Thus this code requires twice the bandwidth. The codes are shown in Figure 8. Many other improved codes are now available.

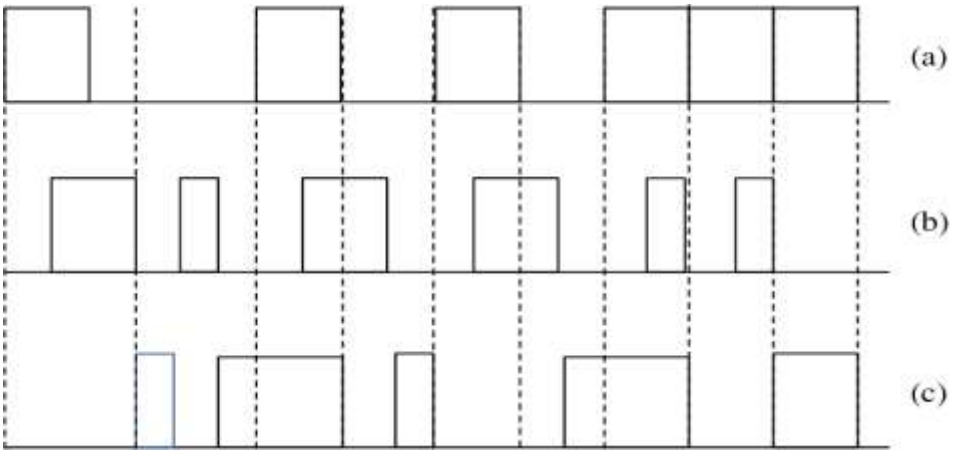

Fig 8: Some of the modulation codes used in optical communication

6.4 System performance

If there is a random reception of unbiased digital data in the optical form, the quantity of interest is the average power in the optical signal and there has to be some minimum average power required in the signal for its reliable detection in the optical domain. Let, P_1 be the average incident power onto the photo-detector when logic 1 is received and P_0 be the average power incident onto the detector when logic 0 is received. Also, let I_1 and I_0 be the generated photo-currents corresponding to the two levels 1 and 0 respectively. Without compromising any generality, it can be assumed that $P_0 = 0$ such that $I_0 = 0$.. If R be the responsivity of the photo-detector then, $I_1 = RP_1$ and $I_0 = RP_0 = 0$. The average power received is given by $P_1/2$. The measure of the noise in the reception of the two logic levels 0 and 1 can be ascertained from the variances in the generated photo-current in the two levels. For the logic 0 reception, there is no incident power and the thermal noise component dominates the noise component in the output signal of the photo-detector. So, the total variance in the 0 level is $\sigma_0^2 = \sigma_T^2$, where σ_T^2 is the variance that characterizes the thermal noise component in the reception. For the logic 1 level, the noise component in the output signal

from the photo-detector is composed of two types of noise- shot noise and thermal noise. Therefore, the total noise variance σ_1^2 is the sum of the variances of shot noise and thermal noise. If the average power of the received signal is large, however, the thermal noise becomes almost negligible in comparison to the shot noise. At low optical power level operation, the average power required to achieve the desired BER is directly proportional to the square root of the bandwidth of operation. Since bandwidth is directly proportional to the data rate of transmission, as the data rate of information transmission increases, the minimum power required to achieve the desired BER also increases. However, this increase is not rapid because the power varies as the square root of the bandwidth.

6.5 Long haul fiber optic system

Telecommunication applications can be broadly classified into two categories: long-haul and short-haul, depending on whether the optical signal is transmitted over relatively long or short distances compared with typical intercity distance. Whereas, short-haul telecommunication applications operate at low bit rates and cover intracity distances of less than 10 km , long-haul telecommunication systems cover several thousand km of distances as in underwater communication. Long-haul systems require high-capacity trunk lines and the optical signal is regenerated electronically using repeaters at regular intervals of 100-200 km, thus enabling the transmission at higher bit rates. Moreover, transmission distances of thousands of km can be enhanced by using optical amplifiers in fiber-optic communication systems.

Long haul communication systems are characterized by a longer trunk distances between users (includes interstate, nationwide, or worldwide distances), higher traffic volumes and densities, large-size switching centers

and central offices, automatic switching for handling calls and messages without operator assistance.

Optical fiber technology has emerged as the preferred technological choice in terms of reliability and cost-effectiveness for Long-haul high-capacity networks. The optical fibers are optimized for high data transmission rate catering to connecting long-distant cities some hundreds to thousands of kilometers. Due to attenuation and dispersion, the transmitted signal amplitude may fade with the distance traversed. So repeaters which consist of amplifiers are spaced equally along the length of a long-haul transmission line to amplify and boost the basic signal strength.

7 Fiber optic networks

The term optical networks or better photonic networks denotes high capacity information communications networks based on photonics technologies and optical components that can provide capacity, provisioning, routing, grooming, or restoration at the wavelength level. The use and application of such networking will reduce cost per transmitted bit per km compared to other long-distance networking technologies, like wire-less networking, coaxial cable/ power-lines-based wire-line networking.

Optical networking solutions span the full spectrum of transport networks from the core backbone and metro down to the access network domains. High bitrate data traffic covering long distances are the characteristics of backbone and metro networks, where photonics networking is dominant. The access network carries different kinds of data streams to and from small units, which are multiplexed/demultiplexed in nodes having fixed back-hauling connections to the transport core network. The use of photonics networking has started its expansion to the access network segment as well.

Two innovations in the optical transmission of information led to the use of multiple channels of light, or wavelengths which could be multiplexed together onto a single fiber. These are wavelength division multiplexing (WDM) techniques and the use of an erbium-doped fiber amplifier (EDFA). Instead of using one amplifier per wavelength, EDFA allows amplifying all wavelengths carried on a fiber.

Fiber network follows general network topologies used in electronics and computer communication networks. It is discussed in nutshell as communication networks consist of sub-networks having different topologies:

1. Point-to-point link topology: It refers to a communications connection between two nodes/stations or endpoints.
2. Star topology: It consists of a star coupler that splits the incoming power into a number of outputs in a star network. The coupler may be of active or passive type depending on whether the data is transmitted to only a specified node/station or all nodes of the network. Hence information passed by one node is passed to another node/station through the coupler.
3. Bus topology: All nodes/stations are connected to the bus. If a signal is transmitted by one node/station, it is transmitted to all other nodes/stations connected to the bus. The transmission may be both ways along the bus.
4. Ring topology: All nodes/stations are connected point-to-point in a ring like manner through optical couplers.

Figure. 9 shows the various network topologies. However, The concept of an all-optical node has been promoted, where the key component is the all-optical switch. Such a device has all-optical interfaces and switches the various wavelengths in the optical domain. Thus, those wavelengths

carrying bypass traffic can remain in the optical domain through the node. All-optical nodes allow enables the removal of a tremendous amount of electronics from the network.

Depending on the advancement of technologies fiber optic networks are divided into two generations:

1. The first-generation network operates on a single wavelength per fiber and is opaque, that is signal in a path is regenerated by repeaters. All signal-switching and processing functions are implemented in the electronic layer. The technology uses fiber distributed data interface (FDDI) and synchronous optical network and synchronous digital hierarchy (SONET/SDH). This framework has standardized line rates, coding schemes, bit-rate hierarchies, and functionality. Types of network elements and network architectures are also standardized.

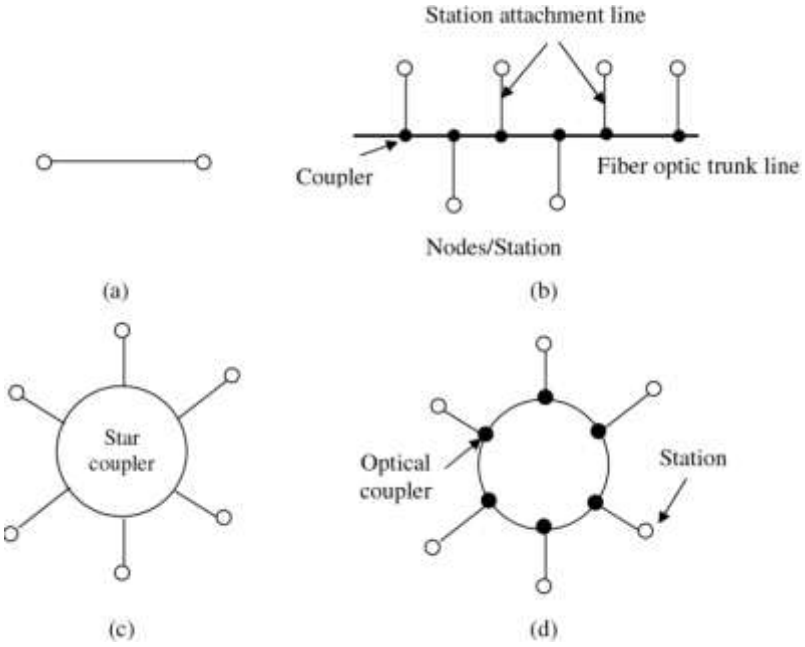

Fig. 9: Various network topologies (a) Point-to-point (b) Bus (c) Star and (d) Ring type.

2. Second generation network utilizes wavelength division multiplexing (WDM) technologies. Backbone core and metro optical networks rely heavily on high-capacity optical transmission links utilizing WDM. Besides offering large transmission capacities per optical fiber, second-generation systems have enabled the realization of wavelength-routed networks with the use of either electronic or optical switching nodes. Multi-wavelength optically routed networks are also characteristics of second-generation systems.

The FDDI scheme uses two fiber pairs, each operating at 100 Mbits/sec where the data bits are coded as bit-patterns and is relatively expensive. FDDI is commonly used at the internet service provider (ISP) peering points that provide interconnections between ISPs. FDDI can support 62.5/125 μm, 50/125 μm, and 100/140 μm multimode fiber sizes with a maximum transmission distance of 2 Km. FDDI also supports the use of single-mode fiber of 8/125 μm, 9/125 μm, and 10/125 μm having a transmission distance of up to 40 Km. Photonic transmitters in the wavelength range 850 nm, 1300 nm, and 1550 nm are used. In general, FDDI uses the ring network topology, as seen in Figure.10. This has two-fiber ring pairs between nodes or workstations (WS) in a node-to-node ring network topology. One of the ring pairs serves as the primary ring and is active while the other is a secondary ring that is kept on hold. In the event of a fiber-break, both the rings are put to use as seen in Figure.10(b).

SONET is used in North America, whereas the SDH network is used in Europe, Japan, and the rest of the world. The transmission bit rate of the (FDDI) network and (b) Use of primary and secondary fibers in case of a fiber break in the FDDI ring.

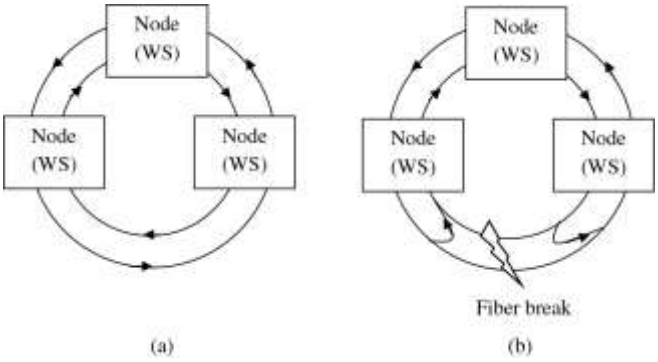

Fig 10 : (A) a two-fiber ring pair in Fiber Distributed Data Interface (FDDI) network and (b) Use of primary and secondary fibers in case of a fiber break in FDDI ring.

basic SONET signal is $51.84\,MB/sec$, whereas the basic SDH rate is $155.52MB/sec$ and is called the synchronous transport module level 1 (STM-1). The SONET/SDH network topologies or configurations may be a

1. Point-to-point topology: In this topology, the nodes may be terminal multiplexers (TM) or line terminating equipment (LTE)
2. Linear topology: In this, the add/drop multiplexers (ADM) are inserted between TM in point-to point-links.
3. Ring topology: The nodes may be accessed through unidirectional path-switched rings (UPSRs) or bidirectional line-switched rings (BLSRs).

SONET/SDH rings are self-healing rings because the traffic flowing along a certain path can be switched automatically following failure or degradation of the link segment. A SONET/SDH ring can be unidirectional or bidirectional. In self-healing SONET/SDH rings, when a failure occurs in the link due to failure of the transmission or receiver equipment or the fiber breaks, the service is automatically restored using the automatic protection switching (APS) protocol. The restoration time is less than 60 msec. The protection or restoration is possible since the two devices at the nodes are

connected with two different fibers (termed the working and protection fibers) such that when a link failure occurs, the SONET/SDH signal is split and simultaneously transmitted over both fibers. The destination selects the best of the two signals. Protection on a SONET/SDH ring can be at the level of a line or a path.

8 Wavelength division multiplexing (WDM) technologies

The main function of a photonic multiplexer is to couple two or more wavelengths into the same fiber. Optical fibers offer a huge bandwidth (~ 100 THz). In fiber-optic communications, wavelength-division multiplexing (WDM) is a technology that multiplexes several optical carrier signals onto a single optical fiber by using different wavelengths of laser light. The source wavelength may vary between 1530 to 1610 nm. Thus, a number of different peak wavelength optical signals can be transmitted through a single fiber, as shown in Figure.11. WDM allows bidirectional communications over the fiber, as well as enhance the transmission capacity.

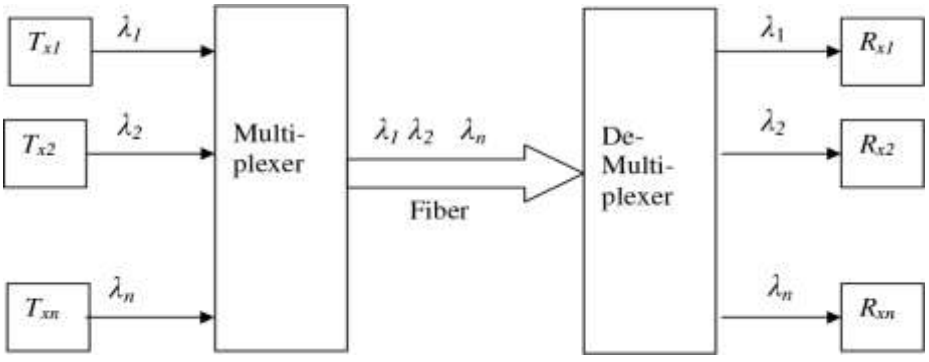

Fig. 11: WDM in an optical fiber communication system.

The transmitter (TX) blocks in the figure are the individual optical transmitters. TX blocks, in themselves, may be multiplexed output of several other transmitter networks thereby forming some sort of a

hierarchical multiplexed architectural system. Also, the transmitter block may consist of a time division multiplexed type of system where the data signals to be transmitted are multiplexed in the time domain. The output signals from these transmitters at their corresponding wavelengths are then multiplexed in the wavelength domain (in accordance with the ITU G.692 standard)by the wavelength multiplexer. The wavelength multiplexer combines all the output signals and combines them to be transmitted along the optical fiber to reach the receiving end. The architecture consists of multiple transmitters and receivers, as far as the type of communication is concerned, though it is still a point-to-point link. Periodic amplifiers and repeaters may be installed along the optical link to establish a secure and the satisfactory optical communication link with the minimum possible BER. At the receiver side, the multiplexed transmitted signal is received and then de-multiplexed by a wavelength de-multiplexer and the respective receivers receive their intended data signals and further processing takes place on these receivers before the signal are delivered to the end-user.

In a WDM system, therefore, bit streams from several transmitters are multiplexed in the wavelength domain together, whereas a wavelength demultiplexer separates channels and feeds them into individual receivers, with channel spacing varying in the range $25 - 100\ GHz$. Modern WDM systems can handle almost 160 signals and can thus expand a basic 10 Gbit/s system over a single fiber pair to over 1.6 Tbit/s. Usually, WDM systems operate on single mode fiber cables having a core diameter of $9\mu m$. But WDM can also be used in multi-mode fiber cables which have core diameters of 50 or 62.5 μm. WDM systems may be either conventional/coarse (CWDM) or dense (DWDM) type. CWDM systems provide up to 8 channels in the C-Band around $1.550\mu m$ silica fibers and DWDM systems provide denser channel spacing in the same transmission

window. Therefore, CWDM in contrast to DWDM uses increased channel spacing to allow less stringent and thus cheaper transceiver designs. In CWDM wideband optical amplification does not occur, limiting the optical spans to several tens of kilometers. DWDM may have 40 channels at 100 GHz spacing or 80 channels with 50 GHz spacing or an even higher number of channels with 12.5 GHz spacing. WDM, CWDM, and DWDM are based on the same concept of using multiple wavelengths of light on a single fiber, but differ in the spacing of the wavelengths, the number of channels, and the ability to amplify the multiplexed signals in the optical space. Some of the advantages of DWDM systems are (a) Capacity for upgradation with minor changes (b) Transparency as the actual timing information of the data is irrelevant to any up gradation in the channel capacity, (c) Wavelength itself can be used as a destination address for routing and (d) Wavelength switching can occur, whenever the required wavelength is non-available due to congestion or other network factors.

8.1 Routing topologies

Routing is the process of selecting the best paths in a network. Wavelength routers are an important component in WDM and are often used in most long-haul networks. Wavelength routing requires photonic switches, cross-connects etc. Wavelength routing networks as shown in Figure.12 are circuit-switched networks. The early development of all-optical networks is typically based on core optical devices in the network nodes which are passive splitters, combiners, and broadcasting stars. Such passive networks support a relatively small number of connections for a given number of wavelengths.

Based on the routing of information delivery at the nodes/stations, the routing schemes as shown in Figure.13 can be (a) unicast, (b) broadcast

(c) any cast (d) Multicast and (e) geo cast. A unicast router delivers information to a single specific node/station, and a broadcast router delivers information to all nodes in the network. Similarly, an any cast system delivers information to anyone out of a group of nodes, typically to the one nearest to the source node in the network. A multicast router provides information to a group of nodes that are interested in receiving the information. A geo cast router delivers information to nodes in a large geographical area.

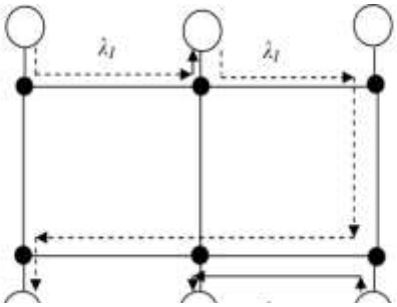

Fig. 12: Wave length routing network

FIGURE 12: Wavelength routing network.

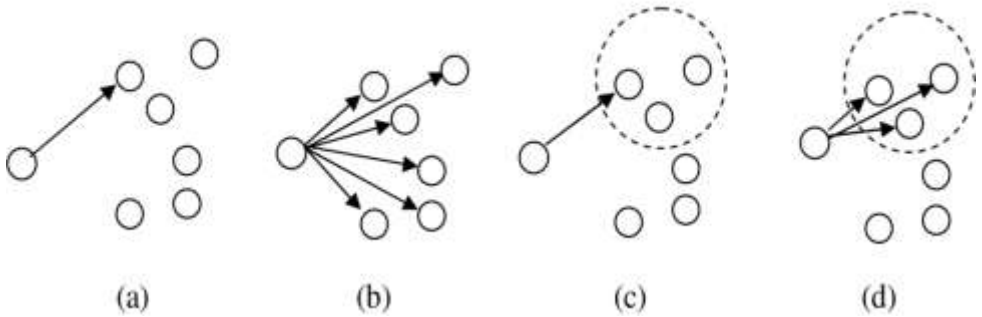

Fig. 13: Routing schemes: (a) Unicast (b) Broadcast (c) Any cast (d) Multicast and (e) Geo cast.

Routing topologies can also be of static/non-adaptive or adaptive type depending on whether the routing tables are constructed manually or automatically. For larger and more complex networks, such manually pre-

computed tables are not feasible, hence the need for dynamic or adaptive routing table arises, which are automatically created as per the need. Adapting routing is carried out by computation of the optimized path length between one node and its neighboring nodes using either of the given algorithms:

Distance vector algorithms: This approach assigns a cost factor to each of the links between each node in the network. The cost is optimized such that a node will send information to another node via the path that results in the lowest total cost. To do this, a node computes the cost factor (or the distance) between all its neighboring nodes. This distance information between a node and all its neighboring nodes and the total cost to each node, and the next hop to send data to get there - makes up the routing table or distance table. Over time, all the nodes in the network will discover the best next hop for all destinations and the best total cost. When one network node fails, the next hop to the failed node is discarded and a new routing-table information is created. These nodes convey the updated routing information to all adjacent nodes, which in turn repeat the process.

Link-state algorithms: For this, a graphical map of the network is needed by each node. To produce its map, each node floods the entire network with information about the other nodes it can connect to and then assembles this information into a map. Using this map, each router independently determines the least-cost path or shortest paths algorithm from itself to every other node. This serves to construct the routing table, which specifies the best next hop to get from the current node to any other node.

Optimized Link State Routing algorithm: A link-state routing algorithm is optimized for mobile ad-hoc networks. Each node discovers 2-

hop neighbor information and elects a set of multipoint relays (MPRs) for routing.

Path vector protocol: Path vector routing is used for inter-domain routing, unlike the other three algorithms. Similar to distance vector routing, one node called the speaker node in each autonomous system acts on behalf of the entire autonomous system. The speaker node creates a routing table and advertises it to neighboring speaker nodes in neighboring autonomous systems. The idea is the same as distance vector routing except that only speaker nodes in each autonomous system can communicate with each other. The algorithm derives its name from the fact that a route is defined as a pairing between a destination and the attributes of the path to that destination.

9 Erbium doped fiber amplifier (EDFA)

In a generic sense, the optical amplifier unit amplifies an optical signal in the same way an electronic amplifier amplifies an electronic signal. An optical amplifier generally consists of an active medium which is excited by a pump source as shown in Figure. 14. The incident optical input signal is then coupled to this active medium via fiber-to-amplifier couplers and the optical signal gets amplified inside this medium by stimulated emissions and the amplified optical output is then recoupled to the optical fiber via another fiber-to-amplifier coupler. When the input optical signal travels through the active medium, the power from the pump gets transferred to the signal power and thus an amplified optical output is obtained.

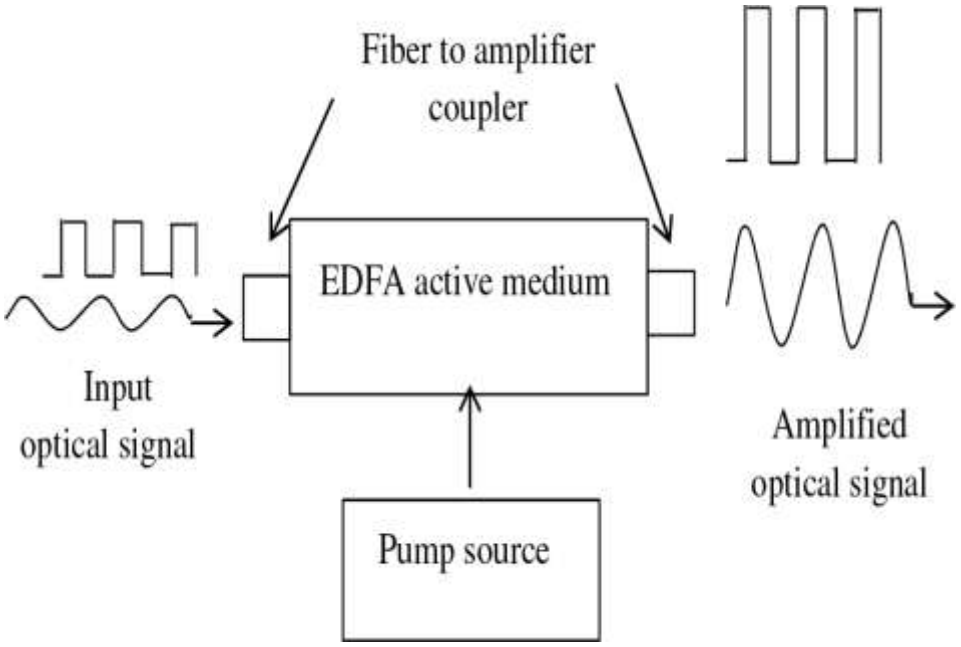

Fig. 14: Generic optical amplifier

Erbium doped fiber amplifier (EDFA) makes use of rare-earth elements as a gain medium by doping the fiber core during the manufacturing process. Amplifier properties such as the operating wavelength and the gain bandwidth are determined by the dopant rather than by the silica fiber, which plays the role of a host medium. Though many dopants are tried, Erbium-doped fiber amplifiers (EDFAs) are found to be suitable as they operate in the wavelength region near 1550 nm. Pumping at a suitable wavelength provides gain through population inversion. The gain spectrum depends on the pumping scheme as well as on the presence of other dopants, such as germania and alumina, within the fiber core. The amorphous nature of silica broadens the energy levels of Er^{3+} into bands. Figure. 15 shows a few energy levels of Er^{3+} in silica glasses.

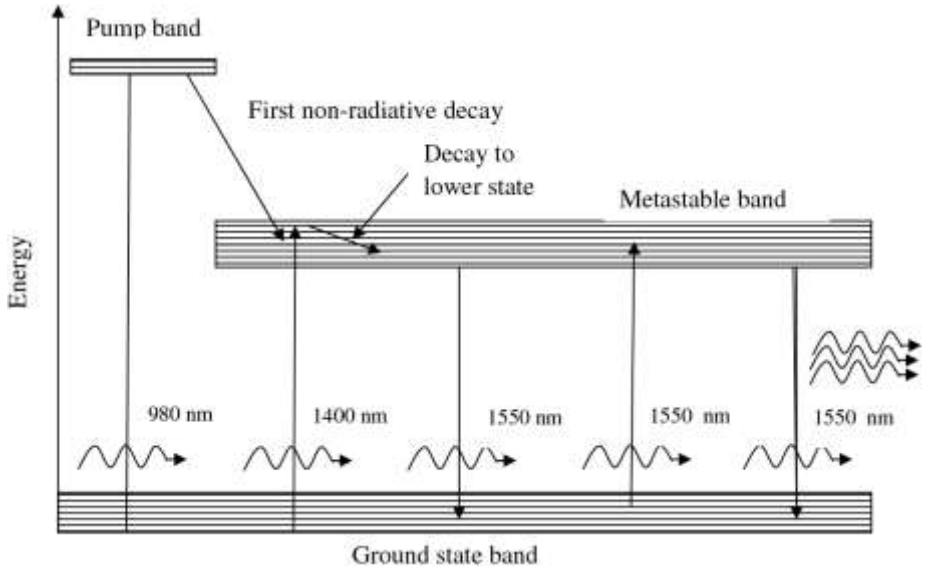

Fig. 15: Energy levels in Erbium

Many transitions can be used to pump an EDFA. Efficient EDFA pumping is possible using semiconductor lasers operating near 980 nm and 1480 nm wavelengths. Once the amplifier material is excited by an appropriate pump source, there are primarily two main types of possible radiations due to downward transitions of the excited electrons- one, which is highly incoherent and occurs naturally, is the spontaneous emission and the other which is coherent and takes place only when stimulated by incident signal photons are the stimulated emission. The stimulated emission is the one that is of importance as far as the optical amplifier function is concerned. However, spontaneous emissions, though can be reduced in number, cannot be eliminated and it is these emissions that lead to a noise component in the optical amplifier output.

The pump source creates and maintains a population inversion condition in the optical amplifier material by pumping it with energy corresponding to a wavelength λ_p of 980nm. The input weak optical signal is combined with λ_p and the two wavelengths travel through the Erbium

core of an optical fiber which acts as the amplifying material. The signal wavelength then gets amplified inside the optical fiber in a similar way as that in the case of a laser and the amplified optical signal is then obtained at the other end. However, the output at the EDFA consists of some portion of the pump wavelength too, which is filtered out using a wavelength de-combiner at the output of the EDFA. The interaction of the pump photon and the signal photon in the EDFA is independent of their relative direction of travel. In other words, if the pumping photons were input to the EDFA from the output end of the device i.e. opposite to the direction of flow of the signal photons, the EDFA would, still, have the same performance characteristics.

For low optical input signal powers, $P_{s(input)} \ll P_{pump}$ and the gain of the amplifier is given by

$$G \approx \frac{\lambda_p}{\lambda_s} \frac{P_{pump}}{P_{s(input)}} \quad \ldots (17)$$

This equation explains the initial high gain of the EDFA at low input signal power levels. The gain however, decreases as the input signal power level rises. The gain of the EDFA is also a function of the length of the Erbium-doped fiber.

The possibilities of photonics integration in enhancing the transport network can be accomplished using the developed WDM photonic integrated circuit module, InP monolithic tunable optical router, high capacity optical switching core, highly scalable integrated optical switch matrix, client interfaces using so-called electro-photonics integrated circuits (EPIC). Further, the entire coherent receiver consists of several photodiodes can be integrated with a photonic integrated circuit (PIC) and the numerous components are all lithographically connected and can much more easily be

path-length matched and balanced. Enhancing the photonic transport networks using some cutting-edge technologies, such as super-continuum light sources and a coherent optical amplifier, have also been demonstrated by researchers.

10 The last mile

The last mile or last kilometer is a phrase widely used in the telecommunications, cable television, and internet industries to refer to the final leg of the telecommunications networks that deliver telecommunication services to retail end-users (customers). More specifically, the last mile describes the portion of the telecommunications network chain that physically reaches the end-user's premises. The last mile is typically the speed bottleneck in communication networks; its bandwidth effectively limits the amount of data that can be delivered to the customer. This is because retail telecommunication networks have the topology of trees, with relatively few high-capacity trunk communication channels branching out to feed many final mile twigs. The final mile links, being the most numerous and thus the most expensive part of the system, as well as having to interface with a wide variety of user equipment, are the most difficult to upgrade to new technology. Although fiber-optic systems excel in high-bandwidth applications, optical fiber has been slow to achieve its goal of fiber to the premises or to solve the last mile problem.

For further reading

1. Optical Fiber Communication : G. Keiser, McGraw Hill, 3rd edition 2000.
2. Fiber Optic Communication Systems: G.P. Agrawal, Wiley, New York, 1997.
3. Optical Fiber Communications: J.M. Senior, Prentice Hall, Englewood Cliffs, NJ, 1992.

4. Optical Fiber Telecommunications, Volume-II : S.E. Miller and I.P. Kainow (Ed.), Academic, New York 1988.
5. Optical Fiber Telecommunications,Volume-III, A and B, I.P. Kainow and T.L. Koch (Eds): Academic, New York 1997.
6. Fiber Optic Communications : J.C. Palais, Prentice Hall, New York, 1998.
7. An Introduction to Fiber Optic Systems; J. Powers, S .Irwin, Chicago. 1997.
8. Optical Networks: R. Ramaswami and K. Sivarajan, Morgan Kaufmann, San Francisco, 1998.
9. Optical Communication Networks: B. Mukherjee, McGraw Hill, New York, 1997.
10. Passive Optical Components for Optical Fiber Transmission: N. Kashima, Artec House, Norwood, MA, 1995.
11. Optical Networks and Their Applications: R. A. Barry, Optical Society of America, Washington, DC, 1998.
12. Design of Optical WDM Networks: B. Ramamurthy, Kluwer Academic, Norwell, MA, 2000.
13. Understanding SONET/SDH and ATM : S. V. Kartalopoulos, IEEE Press, Piscataway, NJ, 1999.
14. Optical Networking with WDM: M. T. Fatehi and M. Wilson,McGraw-Hill, New York, 2002.

———

INFORMATION TO AUTHORS

Manuscripts should represent results of original works on theoretical physics or experimental physics with theoretical background or on applied mathematics. Letters to the Editor and Review articles in emerging areas are also published. Submission of the manuscript will be deemed to imply that it has not been published previously and is not under consideration for publication elsewhere (either partly or wholly) and further that, if accepted, it will not be published elsewhere. It is the right of the Editorial Board to accept or to reject the paper after taking into consideration the opinions of the references.

Manuscripts may be submitted in pdf/MS word format to **admin@citphy.org or susil_vcsarkar@yahoo.co.in** Online submission of the paper through our **website: www.citphy.org** is also accepted. The file should be prepared with 2.5 cm margin on all sides and a line spacing of 1.5.

The title of the paper should be short and self-explanatory. All the papers must have an abstract of not more than 200 words, the abstract page must not be a part of the main file. Abstract should be self-contained. It should be clear, concise and informative giving the scope of the research and significant results reported in the paper. Below the abstract four to six key words must be provided for indexing and information retrieval.

The main file should be divided into sections (and sub-sections, if necessary) starting preferably with introduction and ending with conclusion. Displayed formula must be clearly typed (with symbols defined) each on a separate line and well-separated from the adjacent text. Equations should be numbered with on the right-hand side consecutively throughout the text. Figures and Tables with captions should be numbered in Arabic numerals in the order of occurrence in the text and these should be embedded at appropriate places in the text. Associated symbols must invariably follow SI practice.

References should be cited in the text by the Arabic numerals as superscript. All the references to the published papers should be numbered serially by Arabic numerals and given at the end of the paper. Each reference should include the author's name, title, abbreviated name of the journal, volume number, year of publication, page numbers as in the simple citation given below :

For Periodicals : Sen, N. R. - On decay of energy spectrum of Isotopic Turbulence, 1. Appl. Phys. **28,** No. 10, 109-110 (1999).

1. Mikhilin, S. G. - Integral Equations, Pergamon Press, New York (1964).
2. Hinze, A. K. - Turbulence Study of Distributed Turbulent Boundary Layer Flow, Ph. D, Thesis, Rorke University (1970).

The corresponding author will receive page proof, typically as a pdf file. The proof should be checked carefully and returned to the editorial office within two or three days. Corrections to the proof should be restricted to printing errors and made according to standard practice. At this stage any modifications (if any) made in the text should be highlighted.

To support the cost of publication of the journal, the authors (or their Institutions) are requested to pay publication charge ₹ 200/- per printed page for authors of Indian Institutes and US$ 20 for others. Publication charges to be sent directly to **CALCUTTA INSTITUTE OF THEORETICAL PHYSICS, 'BIGNAN KUTIR', 4/1 MOHAN BAGAN LANE, KOLKATA-700004, INDIA.**

A pdf of the final publisher's version of the paper will be sent to the corresponding author.

All communications are to be sent to the Secretary, Calcutta Institute of Theoretical Physics, 'BignanKutir', 4/1, Mohan Bagan Lane, Kolkata-700004, India. E-mail:susil_vcsarkar@yahoo.co.in

For details please visit our website www.citphy.org

PUBLICATIONS
OF
CALCUTTA INSTITUTE OF THEORETICAL PHYSICS
"BIGNAN KUTIR"
4/1, Mohan Bagan Lane, Kolkata-700 004, India
Phone : +91-33-25555726

INDIAN JOURNAL OF THEORETICAL PHYSICS (ISSN : 0019-5693)
Research Journal containing Original Papers, Review Articles and Letters to the Editor is published quarterly in March, June, September and December and circulated all over the world.

Subscription Rates
₹ 1500 per volume (for Bonafide Indian Party)
US$ 350 (for Foreign Party)

Back Volume Rates
₹ 1500 per volume (for Bonafide Indian Party)
US$ 350 per volume or Equivalent Pounds per volume

Books Written by Prof. K. C. Kar, D. Sc.

- **INTRODUCTION TO THEORETICAL PHYSICS [Vol. I and Vol. II (Acoustics)]** Useful to students of higher physics
  Price :₹ 60 or US $ 10 per volume
- **WAVE STATISTICS : Its principles and Applications [Vol. I and Vol. II]** Useful to Post Graduate and Research students
  Price :₹ 80 or US $ 12
- **STATISTICAL MECHANICS : PRINCIPLES AND APPLICATIONS [Vol. I and Vol. II]** Useful to Advanced students of theoretical Physics
  Price :₹ 120 or US $ 15
- **A NEW APPROACH TO THE THEORY OF RELATIVITY [Vol. I and Vol. II]** Useful to Post Graduate and advanced students
  Price :₹ 50 or US $ 8

Order may be sent directly to Calcutta Institute of Theoretical Physics
"BignanKutir", 4/1, Mohan Bagan Lane, Kolkata-700 004, India